Patient-derived colon epithelial organoids reveal lipid-related metabolic dysfunction in pediatric ulcerative colitis

Babajide A. Ojo[1,2], Lyong Heo[3], Sejal R. Fox[4], Amanda Waddell[5,6], Maria E. Moreno-Fernandez[5,7], Marielle Gibson[1,2], Tracy Tran[1,2], Ashley L. Dunn[1,2], Essam I.A Elknawy[1,2], Neetu Saini[8], Javier A. López-Rivera[1,2], Senad Divanovic[5,6,9], Vinicio A. de Jesus Perez[10], Michael J. Rosen[1,2,#]

[1] Division of Pediatric Gastroenterology, Hepatology, and Nutrition, Stanford University School of Medicine, Stanford, CA, USA

[2] Center for IBD and Celiac Disease, Stanford Medicine Children's Health, Palo Alto, CA, USA

[3] Stanford Center for Genomics and Personalized Medicine, Stanford University, Palo Alto, CA, USA

[4] Applied Gene and Cell Therapy Center, Cincinnati Children's Hospital Medical Center, Cincinnati, OH, USA

[5] Department of Pediatrics, University of Cincinnati College of Medicine, Cincinnati, OH, USA

[6] Division of Immunobiology, Cincinnati Children's Hospital Medical Center, Cincinnati, OH, USA

[7] Division of Gastroenterology, Hepatology, and Nutrition, Cincinnati Children's Hospital Medical Center, Cincinnati, OH, USA

[8] Division of Pediatric Hematology, Oncology, Stem Cell Transplantation and Regenerative Medicine, Stanford University School of Medicine, Palo Alto, CA, USA

[9] Center for Inflammation and Tolerance, Cincinnati Children's Hospital Medical Center, Cincinnati, OH, USA

[10] Division of Pulmonary and Critical Care Medicine, Department of Medicine, Stanford University, Stanford, CA, USA

[#] Address correspondence to Michael J. Rosen, MD, MSCI, Division of Gastroenterology, Hepatology, and Nutrition, Department of Pediatrics, Stanford University, Stanford, CA (rosenm@stanford.edu)

Competing interests: The authors have no competing interests to disclose.

Abstract

Ulcerative colitis (UC) is associated with epithelial metabolic derangements which exacerbate gut inflammation. Patient-derived organoids recapitulate complexities of the parent tissue in health and disease; however, whether colon organoids (colonoids) model the metabolic impairments in the pediatric UC epithelium is unclear. Here, we developed colonoid lines from pediatric patients with endoscopically active UC, inactive UC, and those without endoscopic or histologic evidence of colon inflammation (non-IBD controls) to interrogate functional metabolic differences in the colon epithelia. We demonstrate that colonoids from active UC patients exhibit hypermetabolic features and cellular stress, specifically during differentiation. Hypermetabolism in differentiating active UC colonoids was driven, in part, by increased proton leak, and supported by enhanced glycolytic capacity and dysregulated neutral lipid accumulation. Transcriptomic and pathway analyses indicated a role for PPAR-α in lipid-induced hypermetabolism in aUC colonoids, which was validated by PPAR-α activation in non-IBD colonoids. Accordingly, limiting neutral lipid accumulation in active UC colonoids through pharmacological inhibition of PPAR-α induced a metabolic shift towards glucose utilization, suppressed hypermetabolism and chemokine secretion, and improved markers of cellular stress and epithelial differentiation. Taken together, we reveal a role for lipid-related metabolic dysfunction in the pediatric UC epithelium and support the advancement of colonoids as a preclinical human model for testing epithelial-directed therapies against such metabolic dysfunction.

48 **Main**

49 The restoration of normal intestinal epithelial function is critical for colon mucosa healing in inflammatory
50 bowel diseases (IBD)[1,2]; however, current therapies predominantly target the immune system. As such, only
51 20-30% of patients achieve mucosal healing with today's therapies[3–6]. Ulcerative colitis (UC) is an IBD
52 subtype characterized by the continuous chronic inflammation of the colon mucosa, extending proximally
53 from the rectum[7]. Pediatric UC is marked by more severe and extensive disease than adult UC.[7–11].
54 Achieving mucosa healing is one of the best predictors of sustained disease remission.[11–13] Studies that
55 enhance our understanding of the human intestinal epithelial function in health and disease may advance
56 epithelial-directed therapies in pediatric UC.
57
58 Systemic and local dysregulation of metabolism is a hallmark of inflammation in human IBD[14,15]. Direct
59 investigation of the inflamed human colon tissue in UC has proposed several metabolic impairments in UC,
60 including impaired mitochondrial respiratory chain complex activity, enhanced epithelial mitochondria
61 fission, deficient butyrate metabolism, and reduced epithelial mitochondrial membrane potential[16–19]. This
62 may be critical to the course of disease since mitochondrial activity regulates several aspects of epithelial
63 cellular homeostasis, including the maintenance of energetic balance, adequate reactive oxygen species
64 (ROS) production, and regulating pro-inflammatory responses[20]. However, the cellular mechanisms
65 underlying UC epithelial metabolic dysfunction are not known. Such a deeper understanding may reveal
66 novel epithelial targets to promote mucosal healing.
67
68 The development of epithelial-directed therapies in UC is hindered by a lack of human preclinical models of
69 the diseased epithelium. Over the last decade, advances in organoid biology have grown their promise as
70 human pre-clinical models of disease[21]. In particular, patient-derived adult stem cell organoids are capable
71 of self-organizing into structural and functional models that may reflect the cell and molecular complexities
72 of parent tissues[22]. In UC, patient-derived colon organoids (colonoids) may reflect disease-specific
73 disparities compared to healthy colonoids including alterations in transcription, epigenetics, and somatic

74 gene mutations[23–27]. Despite the promise of intestinal organoids in understanding human intestinal
75 diseases, they have not been used to interrogate the metabolic nature of disease in pediatric UC.
76
77 In this study, we used mucosal biopsy-derived colonoids to understand the metabolic features of colonoids
78 from non-IBD, active, and inactive pediatric UC patients before and during differentiation. We report an
79 inefficient bioenergetic response to differentiation in colonoids from active UC patients characterized by
80 enhanced oxygen consumption and proton leak. UC epithelial metabolic dysfunction was associated with
81 impaired differentiation, and increased cellular stress and chemokine secretion. Differentiating active UC
82 colonoids exhibited increased neutral lipid accumulation and transcriptomic evidence of heightened lipid
83 metabolism. We identified a PPAR-α causal network explaining differential gene expression in active UC
84 colonoids. Accordingly, inhibition of PPAR-α reduced aberrant neutral lipid accumulation, hypermetabolism,
85 cellular stress, and chemokine secretion and improved markers of differentiation in active UC colonoids.
86
87 **Results**
88
89 Derivation of pediatric colon organoids

90 We obtained rectal biopsies from pediatric patients undergoing clinically-indicated colonoscopies (see
91 **Supplementary Table 1** for patient demographics). We dissociated fresh rectal biopsies and removed
92 epithelial cells under a dissecting microscope before culturing and expansion in organoid growth medium
93 (OGM, Extended Data Fig. 1a). We observed enhanced recovery of non-differentiated spheroids from
94 biopsies obtained from non-IBD controls compared to those from active UC (aUC). Control spheroids were
95 sufficiently mature for passaging and expansion by 7 days (Extended Data Fig. 1b), whereas aUC
96 spheroids required 10-14 days. After the extended growth period, fully established aUC spheroids were
97 morphologically comparable to controls and maintained similarity after multiple passages and a freeze-thaw
98 cycle (Extended Data Fig. 1c,d). The timeline and morphology of spheroids generated from inactive UC
99 (iUC) biopsies (patients with endoscopic healing from active disease) were similar to that of biopsies from
100 non-IBD patients (data not shown). To compare the regenerative capacity of spheroids post

101 cryopreservation from each patient group, we digested eight control and aUC spheroid lines into single cell
102 suspensions and measured spheroid diameter after 6 days in OGM. We found no differences in the
103 spheroid diameter between control and aUC spheroids (Extended Data Fig. 2a,b). Overall, we had a 93%,
104 82%, and 89% success rate in generating stable spheroids from colon biopsies obtained from control, aUC
105 and iUC patients, respectively.
106
107 Colonoids from active UC patients exhibit impaired differentiation and hypermetabolism

108 Due to the indifference in spheroid morphology, we wondered whether control and aUC spheroids had
109 analogous metabolic profiles. Hence, we subjected eight individual spheroid lines each from control and
110 aUC patients to extracellular flux analysis to measure the oxygen consumption rate (OCR) at baseline and
111 in response to mitochondrial inhibitors (Extended Data Fig. 2c,d). We found no differences in basal OCR
112 and OCR due to maximal respiration, proton leak, ATP-linked respiration, and non-mitochondrial respiration
113 (Extended Data Fig. 2d). Analysis of mitochondrial mass (mtMass) by fluorescence showed that the
114 undifferentiated control and aUC spheroids had similar mtMass (Extended Data Fig. 2e). Similarly, we
115 analyzed extracellular LDH release into the medium – a marker cellular cytotoxicity – and found no
116 differences in LDH release between control and aUC spheroids (Extended Data Fig. 2f). These results
117 suggest that control and aUC spheroids are morphologically and metabolically similar in their
118 undifferentiated states.
119
120 We then sought to examine the morphology and metabolic profiles of control and aUC spheroids during
121 differentiation. After 3 days in the differentiation condition, we observed morphologic differences between
122 aUC and control differentiating colon organoids (hereafter referred to as colonoids) as more aUC colonoids
123 remained in their cystic morphology compared to the largely budded structures of control colonoids (Fig.
124 1a,b). Further differentiation up to 7 days resulted in visibly reduced survival in aUC colonoids compared to
125 controls (Extended Data Fig. 2g). Apart from morphological features, complementary means to assess
126 differentiation of adult stem cell-derived organoids include their multipotency into mature cell types[28]. Thus,
127 we determined the gene expression of the secretory lineage progenitor, *ATOH1,* (ref: Yang et al, 2001), the

128 enteroendocrine cell marker, *CHGA* (ref), and the crypt-based goblet cell marker of the colon, *WFDC2*[29,30],
129 in C and aUC before and after 3-day differentiation (i.e spheroids vs colonoids). None of the examined
130 markers were significantly different in the control and aUC spheroids (Extended Data Fig 2h,i; Fig. 1c). As
131 expected, *ATOH1* and *CHGA* were upregulated in both control and aUC colonoids compared to their
132 respective undifferentiated spheroids (Extended Data Fig. 2h,i). In aUC colonoids, there was a failure to
133 upregulate WFDC2, consistent with the phenomenon of goblet cell depletion in UC (Fig. 1c)[29]. Furthermore,
134 there was also a reduction in upregulation of CHGA with differentiation as compared to control colonoids
135 (Extended Data Fig. 2i).
136
137 Following the evidence of impaired differentiation in aUC colonoids, we examined whether the metabolic
138 profiles of control and aUC colonoids diverged during the early stages of differentiation. We analyzed OCR
139 in eight patient-derived colonoids per group after 3-day differentiation (Fig. 1d,e). We found a 22% elevation
140 of basal OCR in aUC colonoids compared to the controls. In addition, we found a 75% significant elevation
141 in median OCR due to proton leak in aUC colonoids compared to control, with a non-significant increase in
142 non-mitochondrial and ATP-linked OCR compared to control colonoids (Fig. 1f). The observation that proton
143 leak explained much of the higher oxygen consumption in aUC colonoids suggested mitochondrial
144 inefficiency in aUC. Hence, we measured total ATP and found no significant difference in total cellular ATP
145 between aUC and control colonoids (Fig. 1g). Colon epithelial cells from treatment-naïve UC patients exhibit
146 lower mitochondrial membrane potential (MMP)[19], and we observed a similar reduction in MMP in aUC
147 colonoids compared to controls (Fig, 1h). In line with the hypermetabolic patterns in aUC colonoids, we
148 observed a significant elevation of mtMass during differentiation compared to controls (Fig. 1i).
149 Correspondingly, we found significant increases in mitochondrial ROS levels and LDH release in aUC
150 colonoids compared to control, suggesting that hypermetabolism in aUC colonoids is accompanied by
151 enhanced oxidative stress and cytotoxicity (Fig. 1j,k). Taken together, these data suggest a metabolic
152 inefficiency in aUC colonoids at the early stages of differentiation which may contribute to oxidative stress
153 and cytotoxicity.
154
155 Colonoids from inactive UC patients recall features of hypermetabolism upon inflammatory exposure

156 Following the dysregulated metabolic profile observed in aUC colonoids, we asked whether colonoids from
157 inactive UC (iUC) patients, those on treatment with no endoscopic disease activity, were metabolically
158 distinct from control colonoids. First, we observed no morphological differences between control and iUC
159 colonoids during differentiation (Extended Data Fig. 3 a,b). The bioenergetic profiles of control and iUC were
160 similar after a 3-day differentiation as we observed no differences in basal OCR, proton leak, maximal
161 respiration, and ATP-linked OCR; however, non-mitochondrial OCR was higher in iUC compared to control
162 colonoids (Extended Data Fig. 3c,d). Accordingly, and similar to our observation in aUC colonoids, we
163 observed enhanced ROS in iUC colonoids compared to control colonoids, suggesting that ROS generation
164 in our colonoids is not solely coupled to hypermetabolism.
165
166 Since biopsies for aUC colonoids were obtained from inflamed epithelial regions, we wondered whether
167 prior exposure to inflammation *in vivo* may explain the hypermetabolic nature of aUC colonoids *in vitro*. To
168 model this, we reasoned that the pre-exposure of spheroids to inflammation may recapitulate
169 hypermetabolic features in control and iUC colonoids during differentiation. Thus, before differentiation, we
170 exposed control and iUC spheroids to a modified inflammatory cocktail (40 ng/mL TNFa, 20 ng/mL IL1b,
171 and 500 ng/mL flagellin) previously suggested to re-induce the inflammatory nature of UC *ex vivo*[25]
172 (Extended Data Fig. 3f). We observed that unlike control colonoids, iUC spheroids showed reduced budded
173 morphology after a 3-day differentiation when pre-exposed to the inflammatory cocktail. (Extended Data Fig.
174 3g). We observed pre-exposure with the inflammatory cocktail led to enhanced mtMass in iUC but not
175 control colonoids (Extended Data Fig. 3h). Correspondingly, we found a significant increase in basal OCR
176 in iUC colonoids pre-exposed to the inflammatory cocktail compared to vehicle and exposed control.
177 However, there were no significant effects on maximal OCR and proton leak (Extended Data Fig. 3i,j).
178 Collectively, these data suggest that iUC spheroids are more susceptible to inflammatory challenge and this
179 leads to a partial recapitulation of aUC-related enhanced respiratory phenotypes during differentiation.
180
181 Metabolic uncoupling contributes to hypermetabolism in aUC colonoids

182 The proton leak and resulting metabolic inefficiency observed in aUC colonoids during differentiation may
183 be indicative of enhanced uncoupling of mitochondrial respiration[31]. Thus, we hypothesized that
184 endogenous mitochondrial uncoupling proteins would be upregulated in aUC compared to control. First, we
185 analyzed public bulk RNA-seq datasets from the RISK study (GSE117993)[32] and PROTECT Pediatric IBD
186 inception cohort studies (GSE109142)[19] and found that RNA for uncoupling protein 2 (*UCP2*) is the
187 dominant uncoupling protein RNA expressed in non-inflamed rectal tissue from non-IBD control patients
188 (Extended Data Fig. 4a). Rectal gene expression data from 56 and 206 UC patients in the RISK and Protect
189 Studies, respectively, showed that *UCP2* is significantly upregulated in the rectal mucosa of pediatric UC
190 patients compared to controls (Extended Data Fig 4b,c). In our patient-derived colonoid samples, we
191 confirmed enhanced UCP2 expression at the mRNA and protein levels (Extended Data Fig 4d).
192 Immunofluorescence imaging showed the coexpression of UCP2 protein with the mitochondrial marker
193 COX4, suggesting enhanced presence of UCP2 in the mitochondria during differentiation (Extended Data
194 Fig 4e).
195
196 To test whether metabolic uncoupling was sufficient to induce the altered colon epithelial differentiation and
197 metabolism observed aUC, we added a low-dose Fccp (protonophore that uncouples mitochondrial
198 OXPHOS), into the medium throughout a 3-day differentiation of control colonoids (Extended Data Fig. 4f).
199 Paired analysis showed a significant elevation of basal OCR and OCR due to maximal respiration, proton
200 leak, non-mitochondrial respiration, but also significantly increased ATP-linked respiration, suggesting that
201 the healthy colonoids may overcome chemical uncoupling to maintain ATP levels (Extended Data Fig. 4g,h).
202 Still, we observed elevated mtMass and mitochondrial ROS levels in Fccp-treated colonoids compared to
203 controls suggesting an increase in mitochondrial and oxidative stress during differentiation (Extended Data
204 Fig. 4i,j). In contrast, we did not see an increase in LDH release to suggest uncoupling alone induced
205 cytotoxicity (Extended Data Fig. 4k). Finally, we observed that Fccp uncoupling during differentiation did not
206 impact colonoid morphology or *WFDC2* gene expression (Extended Data Fig 4l-n). These data suggest that
207 upregulation of UCP2 and mitochondrial uncoupling likely contribute to hypermetabolism and oxidative
208 stress in aUC colonoids, but may be insufficient to impair differentiation or induce cytotoxicity.
209

210 Active UC colonoids exhibit an altered transcriptional profile and upregulated chemokine secretion

211 To understand transcriptional changes that may underly altered metabolism and function in aUC colonoids,
212 we conducted bulk RNA-seq on spheroids and colonoids differentiated for 3 days (n= 8 patient lines per
213 diagnosis, passage 5-7). Among 13,884 genes detected in spheroids after quality control, only seven were
214 significantly upregulated (*CYP3A4, KRT23, FLNC, APOL1, DAPP1, TNFSF15, GRHL3*) and four were
215 significantly downregulated (*EVC, NEFH, CDKN1C, SORBS1*) in aUC compared to control undifferentiated
216 spheroids ($Log_2FC \geq \pm 1$, FDR $P \leq 0.1$, Extended Data Fig 5a, Supplementary Table 2). These findings
217 suggest that in conditions promoting stemness, C and aUC spheroids are largely transcriptionally similar in
218 agreement with their metabolic similarity.
219
220 We found that upon differentiation, control and aUC colonoids had divergent transcriptomic profiles (Fig.
221 2a), in line with their distinct metabolic profiles. Specifically, 112 genes were significantly upregulated and 34
222 significantly downregulated ($Log_2FC \geq \pm 1$, FDR $P \leq 0.1$; Supplementary Table 2). The top upregulated
223 genes included well-known MHCII-related genes in active UC[19,33,34], *HLA-DRA, HLA-DMB, HLA-DRB, HLA-*
224 *DMA* (Fig. 2b, Supplementary Table 2); lipid-related genes (*FABP6, ABCA12, and APOL3*); and *CARD6* a
225 member of the caspase recruitment domain family (ref) (Fig. 2b, Supplementary Table 2). Top
226 downregulated genes included those involved in the development of cytoskeletal filaments (*NEFH, KRT12*),
227 goblet cells (*ZG16, WFDC2*), and those involved in cellular development and histone maintenance (*GATA2*
228 and *HIST1H4K*, respectively) (Fig. 2b, Supplementary Table 2). Consistent with the metabolic profile of
229 inactive UC colonoids, only two genes (*HLA-DRA* and *HLA-DMB*) were significantly upregulated in iUC
230 colonoids compared to control colonoids (Supplementary Table 2).
231
232 Chemokines recruit immune cells to the epithelium in UC, where they can incite damage. We observed
233 enhanced expression of chemokine genes involved in the recruitment of macrophages (CCL2), T-cells
234 (CXCL11), neutrophils, (CXCL1), and T- and B-cells (CCL28) in aUC colonoids compared to controls (Fig.
235 2c). Using medium collected during a 2-d differentiation, We confirmed by ELISA of colonoid media after 2
236 days of differentiation that aUC colonoids exhibit increased secretion of these chemokine proteins

237 compared to controls (Fig 2d-f). Due to the contribution of metabolic uncoupling to the hypermetabolism in
238 aUC colonoids (Extended Data Fig. 4), we asked whether metabolic uncoupling was sufficient to induce
239 chemokine secretion in control colonoids during differentiation Indeed, treatment of control colonoids with
240 Fccp during differentiation significantly upregulated the gene and protein secretion of CXCL1, CXCL11, and
241 CCL2 (Extended Data Fig. 4o,p). Thus, molecular events that stimulate metabolic uncoupling during
242 epithelial differentiation in UC may contribute to the chemoattraction of immune cells.
243
244 Active UC colonoids exhibit enhanced glycolytic capacity

245 To begin to understand the cellular underpinnings of hypermetabolism in aUC colonoids, we analyzed our
246 differentially expressed transcriptomic data using functional annotation analysis (Ingenuity Pathway Analysis
247 [IPA])[35] to predict the dominant molecular and cellular functional differences between aUC and control
248 colonoids. IPA implicated carbohydrate metabolism as the top mediator of cellular function during
249 differentiation (Fig. 3a). Other dominant functions include molecules involved in cell death and survival,
250 cellular assembly and organization, cellular development, cellular growth and proliferation, and lipid
251 metabolism (see details of all cellular and molecular functions in Supplementary Table 3).
252
253 Given that carbohydrate metabolism is the top cellular function in our data, we tested whether aUC
254 colonoids exhibited enhanced glycolysis during differentiation. In aerobic glycolysis, pyruvate is produced,
255 which enters the citric acid cycle. In anaerobic glycolysis, pyruvate is converted to lactate. We assessed
256 extracellular acidification rates (ECAR) that result predominantly from lactate secreted as an end product of
257 anaerobic glycolysis[36] by extracellular flux analysis in control and aUC colonoids beginning in a glucose-
258 depleted medium. After glucose injection, we did not observe any differences in ECAR due to anaerobic
259 glycolysis (Fig. 3b,c). However, we observed that aUC colonoids had an enhanced glycolytic capacity and
260 reserve compared to control colonoids after the suppression of OXPHOS by inhibiting mitochondrial
261 complex V (ATP Synthase) with oligomycin[37] followed by inhibition of glycolysis with 2-deoxy glucose (Fig.
262 3b,d-e). Still, non-glycolytic acidification in aUC was significantly higher compared to controls, which
263 suggests other pathways such as CO_2 from the TCA cycle contribute to extracellular acidification[36].

264

265 To complement the results of real-time extracellular flux analysis, we used medium collected over the first 2
266 days of differentiation to measure cumulative extracellular glucose consumption and lactate production
267 during the early process of differentiation. On average, aUC colonoids consumed 4.2 times more glucose
268 from the media and produced 2.8 times more lactate compared to controls (Fig. 3g,h). Collectively, the data
269 indicate that, during the early stages of differentiation, aUC colonoids consume more glucose and exhibit
270 increased capacity for glycolysis which could support the observed hypermetabolism.

271

272 Dysregulated lipid metabolic genes in aUC colonoids

273 Functional annotation analysis of aUC colonoid differential gene expression also identified lipid metabolism
274 as one of the top 10 dominant molecular and cellular functions (Fig. 3a). Upregulated lipid metabolism
275 genes in aUC included those related to fatty acid transport (*FABP6, ABCA12*), apolipoproteins (*APOL1,*
276 *APOL3*), sphingolipids and phospholipid biosynthesis (*SPTLC3* and *DGKG*, respectively), lipid-metabolizing
277 CYPs (*CYPC218*, *CYP3A4*), and lipolysis (*LPL, PLB1, AADAC, LIPA*). The only downregulated lipid-related
278 gene was *ALOX15B*, which plays a role in the generation of specialized pro-resolving lipid mediators in
279 inflammation (Supplementary Table 3, Fig. 4a) [38].

280

281 To confirm that increased expression of these lipid-related genes in aUC colonoids is relevant to the colon
282 epithelium in patients, we examined their expression in other bulk and single-cell RNA-seq UC data sets.
283 First, the PROTECT bulk RNA-seq data from 206 pediatric patients also showed enhanced expression of
284 *ABCA12, APOL3, APOL1, LPL, DGKG,* and *LIPA* in active UC patients compared to controls (Extended
285 Data Fig. 5a). Next, we analyzed a publically available UC single-cell RNA-seq data[39] to evaluate whether
286 inflamed epithelial cells exhibit similar upregulation of lipid-related genes in UC. Compared to healthy
287 samples, a higher proportion of the inflamed samples visibly expressed these identified lipid-related genes
288 including stem cells and other progenitor epithelial lineages (Extended Data Fig. 5b,c). Taken together,
289 these analyses of the complementary organoid, bulk tissue, and single-cell RNA-seq data sets indicate the
290 transcriptomic dysregulation of lipid-related genes in UC is modeled in our colonoids.

291

292 Aberrant lipid accumulation and oxidation in aUC colonoids during differentiation

293

294 Considering the altered expression of lipid metabolic genes in aUC, we sought to determine whether
295 enhanced lipid metabolism contributes to the observed hypermetabolic phenotype. First, we measured the
296 accumulation of BODIPY^{+} neutral lipids in our colonoids before and during differentiation. Consistent with
297 their analogous metabolic states before differentiation, control and aUC spheroids had similar neutral lipid
298 content (Fig. 4b). However, we observed a significant increase in neutral lipid accumulation during
299 differentiation in aUC colonoids compared to their paired spheroids, while control spheroids and colonoids
300 still retained similar neutral lipid content. (Fig. 4b). Furthermore, differentiated aUC colonoids contained
301 elevated lipid content compared to the control colonoids (Fig. 4b,c). Extracellular and intracellular
302 triglycerides, cholesterol esters, and membrane phospholipids are hydrolyzed to free fatty acids, which
303 undergo fatty acid oxidation (FAO) and support OXPHOS. Our bulk RNA-seq data showed an upregulation
304 of 4 lipid hydrolysis genes (*LPL, PLB1, AADAC, LIPA*) in aUC colonoids (Fig. 4a), which is largely similar to
305 the analyzed single-cell RNA-seq data[39] (Extended Data Fig. 5c). Specifically, we observed that lipoprotein
306 lipase (*LPL)* was predominantly overexpressed in differentiating cycling transit amplifying (TA) cells in
307 inflamed samples (Extended Data Fig. 5c). Since TA cells are progenitors that are involved in cell cycle,
308 mitochondrial biogenesis and terminal differentiation into mature epithelial cell types[30,40], we reasoned that
309 for our colonoids to recapitulate *in vivo* lipid metabolic phenotypes, LPL activity would dissipate over time
310 during differentiation. Indeed, a 5-day differentiation protocol showed elevated LPL activity in aUC colonoids
311 compared to control on Day 2, however, by Day 5 of differentiation, LPL activity in both control and aUC
312 dropped to pointedly low levels with no significant difference between groups (Fig. 4d). These data further
313 suggest that active lipid cycling may be overamplified during differentiation in the UC colon epithelium and
314 our pediatric colonoid model of UC may recapitulate these lipid metabolic dynamics similar to the parent
315 tissues from whence they came.

316

317 Given the increased potential for neutral lipid accumulation and lipid hydrolysis in aUC colonoids, we
318 hypothesized that the oversupply of lipids contributes to elevated O_2 consumption in aUC colonoids during

319 differentiation. Thus, we exposed control and aUC colonoids to a nutrient-depleted medium with or without
320 etomoxir, a carnitine palmitoyl-transferase 1a (CPT1a) inhibitor that inhibitis fatty acid oxidation (Fig. 4e).
321 With negligible external sources of metabolic substrates, aUC colonoid mean basal OCR was 78% greater
322 than that of controls (Fig. 4f,g). Etomoxir reduced basal OCR in aUC colonoids to the level of control
323 colonoids (Fig. 4g). Further, etomoxir did not impact maximal respiration (Extended Data Fig. 6a). Etomoxir
324 significantly reduced proton leak in aUC but not control colonoids, suggesting that enhanced FAO drives
325 proton leak in aUC (Fig. 4h). Compared to control colonoids, we observed a significant increase in ATP-
326 linked OCR in aUC colonoids under this nutrient-depleted condition, with a significant decrease in ATP-
327 linked OCR in aUC with etomoxir inhibition (Fig. 4i). Non-mitochondrial respiration was elevated in aUC
328 colonoids compared to control with no effect observed with etomoxir treatment in either group, which
329 suggests that etomoxir specifically modulated mitochondrial respiration in this model (Extended Data Fig.
330 6b). These results indicate that there is enhanced lipid accumulation and oxidation in the differentiating
331 active UC epithelium which is necessary for the hypermetabolic phenotype during differentiation.
332
333 Lipotoxicity precedes *CXCL1* overexpression during colonoid differentiation
334
335 Lipid exposure induces stemness in intestinal progenitor cells[41]; hence, we wondered whether lipotoxicity
336 during colonoid differentiation may contribute to the impaired differentiation and chemokine expression
337 observed in aUC colonoids (Fig. 1c, Fig. 2c). Thus, we exposed control spheroids to BSA-bound palmitic
338 acid (BSA-PA) during the initial 24 hrs of differentiation. We found a dose-dependent increase in the gene
339 expression of the uncoupling protein *UCP2*, fatty acid transporter *FABP6*, and a decrease of the crypt-base
340 goblet cell marker, *WFDC2*[29] (Extended Data Fig. 6c) in response to BSA-PA exposure. Consequently, we
341 hypothesized that lipid-induced stress and toxicity to the colon epithelial progenitors in aUC may contribute
342 to the observed enhanced chemokine production in aUC colonoids under non-stimulated conditions *in vitro*.
343 Hence, we exposed non-IBD colonoids to BSA-PA in ODM for 3 days and continued differentiation without
344 PA until day 5 (Fig. 4k). Compared to control, PA exposure impaired colonoid morphology and induced a
345 significant upregulation of *CXCL1* in all colonoid lines (Fig 4j,m). Overall, these data suggest that fatty acid
346 exposure may impair differentiation and induce inflammation in differentiating colon epithelial cells.

347

348 PPAR-alpha contributes to lipid-induced hypermetabolic stress during colonoid differentiation

349 To understand the regulatory networks that may explain the hypermetabolic nature of differentiating aUC
350 colonoids, we applied Causal Network Analysis of our bulk transcriptomic colonoid data[35]. We identified the
351 PPARA-RXRA network as the most significant causal factor (Fig. 5a). Other notable networks include HIF3A
352 (endogenous lipid sensor[42]), tyrphostin (role in metabolic uncoupling[43]), MLXIPL (role in carbohydrate
353 sensing and glucose-induced lipogenesis[44]), and SH3GLB1 (contributes to lipolysis and lipid droplet
354 clearance[45]).

355

356 We focused on PPAR-α as it regulates a family of genes central to glucose and lipid metabolism[46]. Analyses
357 of epithelial lineage-specific PPARA expression in the scRNA-seq data from treatment-naïve UC colon
358 epithelium[39] showed the upregulation of PPARA majorly in progenitor cells (stem, TA2, cycling TA, secretory
359 TA) in the inflamed and non-inflamed colon epithelial regions compared to healthy samples (Extended Data
360 Fig. 7a). We did not see any differences in *PPARA* mRNA expression in our bulk RNA-seq data between
361 aUC and control colonoids differentiated for 3 days; however, we found an enhanced PPAR-α activity in
362 nuclear extracts from aUC colonoids compared to controls at the early stages (24 hr) of differentiation
363 (Extended Data Fig. 7b).

364

365 Given the upregulation of PPAR-α-induced genes and PPAR-α DNA binding in aUC colonoids, we
366 wondered whether PPAR-α activation is sufficient to induce the observed hypermetabolic phenotype.
367 Treatment of control colonoids with the PPAR-α agonist fenofibrate during differentiation significantly
368 reduced colonoid budded morphology in every patient colonoid line tested (Fig. 5b-d). Consistent with the
369 differentiation pattern in aUC colonoids, we found a significant downregulation of the crypt-base goblet cell
370 marker[29] *WFDC2,* in control colonoids exposed to fenofibrate (Fig. 5e). Fenofibrate enhanced metabolic
371 substrate utilization as we observed increased glucose consumption over two days in every colonoid line
372 compared to untreated control (Fig. 5f). Overall, glucose consumption was not accompanied by significant
373 lactate production suggesting a negligible induction of anaerobic glycolysis (Fig. 5g). Fenofibrate treatment

374 enhanced UCP2 expression during colonoid differentiation (Fig. 5h). Consistent with aUC lipid metabolic
375 phenotypes, we observed a significant accumulation of neutral lipids and enhancement of LPL activity in
376 control colonoids exposed to fenofibrate (Fig. 5i-k). We also observed enhanced mitochondrial mass, and
377 mitochondrial ROS in control colonoids upon fenofibrate treatment (Fig. 5l,m). Following these observations,
378 we hypothesized that fenofibrate treatment during differentiation would result in organoids with a
379 hypermetabolic bioenergetic profile similar to that seen previously in aUC. Indeed, differentiation of control
380 colonoids exposed to fenofibrate resulted in significantly higher basal, maximal, proton leak, and non-
381 mitochondrial OCR with no significant increase in ATP-linked OCR (Fig. 5n,o). Finally, fenofibrate treatment
382 induced LDH release (a marker of cytotoxicity) consistent with our observation in differentiating aUC
383 colonoids (Fig. 1k, Fig. 5p). These findings suggest that there is enhanced PPAR-α activity in active UC and
384 such activity is sufficient to induce to hypermetabolic stress and impair differentiation in colon epithelial
385 cells.
386
387 Pharmacological inhibition of PPAR-α reprograms epithelial metabolism in aUC colonoids

388 Following the observed contribution of PPAR-α activity to lipid accumulation and hypermetabolic stress
389 during differentiation, we reasoned that inhibition of PPAR-α during aUC colonoid differentiation may
390 prevent endogenous lipid accumulation and improve metabolic and cellular stress. We supplemented ODM
391 with the PPAR-α antagonist, GW6471 (GW) during differentiation of aUC colonoids. GW treatment in aUC
392 colonoids suppressed neutral lipid accumulation during differentiation in every colonoid line compared to
393 untreated aUC colonoids (Fig. 6a,b). GW treatment in aUC colonoids also downregulated *LPL* and *UCP2*
394 gene expression (Extended Data Fig. 8a, Fig. 6c). We then determined mitochondrial bioenergetics in aUC
395 colonoids differentiated with or without GW in substrate-enriched medium (10 mM glucose, 1 mM pyruvate,
396 2 mM glutamine). We observed a significant reduction in basal, maximal, proton leak, and ATP-linked OCR
397 in GW-treated colonoids (Fig. 6). Luminescence assay for total cellular ATP showed no significant
398 differences in untreated and GW-treated aUC colonoids. These data suggest that PPAR-α inhibition reduces
399 lipid accumulation and normalizes cellular bioenergetics in active UC colon epithelial cells.
400

401 To test whether PPAR-α inhibition improved UC colon epithelial bioenergetics through altering FAO, we
402 examined the effect of GW on colonoids in the presence or absence of etomoxir. Blockade of FAO with
403 etomoxir did not affect basal OCR in GW-treated aUC colonoids (Fig. 6g,h). Similarly, etomoxir did not have
404 any effect on maximal OCR, proton leak, ATP-linked OCR, or non-mitochondrial OCR in GW-treated aUC
405 colonoids (Extended Data Fig. 8b-e). These data suggest that GW treatment suppressed the
406 hypermetabolic bioenergetic profile of aUC colonoids by reducing FAO. Since GW treatment starved aUC
407 colonoids of lipid-based metabolic substrates during the energy-demanding differentiation, we reasoned that
408 GW may have induced a metabolic switch to the usage of other substrates to sustain differentiation. Hence,
409 we assayed for extracellular glucose and lactate in ODM over 2 days of differentiation in aUC colonoids with
410 or without GW. We observed a significant increase in glucose consumption in all GW-treated aUC colonoid
411 lines compared to their paired untreated aUC colonoids without changes in lactate production, suggesting
412 an increased reliance of glucose as a substrate for OXPHOS (Fig. 6i,j).
413
414 We next examined whether the metabolic reprogramming in aUC colonoids with PPAR-α inhibition impacted
415 cellular health markers. GW treatment in aUC colonoids did not impact mitochondrial mass or mitochondrial
416 ROS levels compared to untreated aUC colonoids (Extended Data Fig. 8f,g). In contrast, GW treatment
417 significantly reduced LDH release (cytotoxicity marker) in every colonoid line compared to untreated aUC
418 colonoids (Fig. 6k). Considering that lipotoxicity contributed to chemokine expression in differentiating
419 colonoids (Fig. 4n), we hypothesized that the prevention of neutral lipid accumulation by GW during
420 differentiation would impact epithelial chemokines secreted in aUC colonoids (Fig. 2d-f). Hence, we
421 collected ODM from colonoids differentiated for 2 or 5 days and found that GW treatment in aUC colonoids
422 significantly suppressed extracellular CXCL1 protein in day 2 and day 5 ODM collected from all colonoid
423 lines tested (Fig. 6l). There was no significant effect of GW treatment on extracellular CXCL11 and a trend
424 toward a reduction in extracellular CCL2 on day 2 ($p=0.053$) while there was no effect on day 5 (Extended
425 Data Fig. 8h,i).
426
427 Considering that aUC colonoids exhibited morphologic evidence of impaired differentiation and
428 corresponding downregulated expression of the crypt-base goblet cell marker, *WFDC2* (Fig. 1a-c), we

429 asked whether the remodeling of colonoid metabolism in aUC with GW treatment impacted differentiation
430 markers. Blinded visual assessment of colonoid morphology showed no consistent impact of GW on
431 colonoid budding (Fig. 6m,n). To complement these findings, we assessed the mRNA expression of
432 stemness markers (*LGR5* and *ASCL2*) and goblet cell markers *WFDC2* and *MUC2*. The expression of
433 stemness markers reduced over time in every aUC colonoid line with GW treatment, with significant
434 downregulation in *ASCL2* (Fig. 8p). *WFDC2* significantly increased in GW-treated colonoid lines compared
435 to untreated aUC colonoids while the increase in *MUC2* expression was not statistically significant (Fig. 8o).
436 Overall, these data suggest that PPAR-α inhibition in aUC colonoids reduces chemokine secretion and
437 augments molecular markers of epithelial differentiation.
438
439 **Discussion**
440
441 Leveraging clinical samples to develop human IBD pre-clinical models is important for determining
442 mechanisms of human disease pathogenesis. We used patient-derived colon epithelial organoids as a
443 human model to study epithelial metabolic dysfunction in pediatric UC. We report profound elevation in
444 oxygen consumption in aUC colonoids during differentiation related primarily to increased proton leak. This
445 hypermetabolic phenotype was associated with increased chemokine secretion, oxidative stress,
446 cytotoxicity, and impaired differentiation. The aUC colonoids showed an elevated capacity for lipid
447 accumulation during differentiation and their hypermetabolic phenotype required FAO. Our data indicate
448 PPAR-α drives altered lipid metabolism and OXPHOS in aUC colonoids and that pharmacological inhibition
449 of PPAR-α normalizes abnormal metabolism, chemokine expression, and differentiation in aUC epithelial
450 cells.
451
452 In our study, colonoids from active UC patients showed increased mitochondrial respiration during
453 differentiation without a concomitant change in ATP levels. The normal colon epithelium is less dependent
454 on highly oxidative processes for energy generation[47,48]. Accordingly, our data in non-IBD control colonoids
455 showed marginal increases in median oxygen consumption during the energy-demanding differentiation
456 process. Hypermetabolism may channel energetic demands towards molecular programs that favor a

457 hypersecretory phenotype[49,50], which may explain the hypersecretion of chemokines in aUC colonoids
458 during differentiation. Furthermore, the oversupply of metabolic substrates may result in hypermetabolism
459 with associated mitochondrial and cellular stress[51]. Cellular dependency on lipids for energy generation is
460 inefficient since the oxidation of lipids consumes energy and induces metabolic uncoupling[52] as observed
461 with increased proton leak and UCP2 expression in our aUC colonoids. This notion is corroborated by our
462 finding of *UCP2* induction in healthy colonoids exposed to palmitic acid. Our transcriptomic and functional
463 data suggest a lipid-related hypermetabolism during differentiation in epithelial aUC colonoids, which may
464 increase the energetic cost of differentiation and contribute to enhanced epithelial cellular stress in aUC.
465
466 The large PROTECT pediatric UC inception cohort study[19] examined rectal mucosa bulk RNA expression in
467 children with active UC and non-IBD controls and found extensive downregulation of genes related to
468 mitochondria and OXPHOS. Several of our findings in colonoids were in line with the PROTECT study
469 tissue data including increased expression of the uncoupling gene UCP2, and multiple lipid-related genes
470 and decreased epithelial MMP in active UC. Notably, the PROTECT study did not examine colon epithelial
471 respiration directly. While we did not observe any significant changes in mitochondrial genes in our aUC
472 colonoids (data not shown), we observed abnormally high mitochondrial respiration in aUC colonoids. In a
473 dextran sodium sulfate (DSS) mouse model of colitis[53], enhanced epithelial OXPHOS activity was reported
474 during the active stage of the disease at day 7 despite the downregulation of some mitochondrial genes.
475 These metabolic and transcriptional disparities in the active epithelium largely resolved to the level of
476 control upon recovery at day 28[53]. It is possible that the downregulation of mitochondrial genes is driven by
477 the inflammatory milieu of the colon mucosa which is absent in the sterile culture of colonoids in our study.
478
479 Our study provided functional evidence of lipid metabolic dysregulation in the pediatric UC epithelium. Few
480 metabolomic and animal studies have suggested the potential contribution of lipid metabolic dysregulation
481 to IBD[54]. In adults, onset of UC is predicted 4 years earlier by upregulated lipid biosynthesis, elongation,
482 and degradation pathways as measured by plasma metabolomics[55]. Elevated fecal fat is apparent in UC
483 patients (as reviewed previously[56]), and lipid dysregulation occurs in the colon tissue of the DSS-induced
484 mouse model of colitis[57]. These studies support our findings as they suggest colon epithelia may be

485 exposed to excess lipid or abnormally process lipid during intestinal inflammation – even before disease
486 onset. Neutral lipid accumulation in lipid droplets may be a cytoprotective mechanism against lipotoxic-free
487 non-esterified fats[58]. Conversely, aberrant lipid accumulation or lipid droplet hydrolysis may trigger
488 lipotoxicity-related pathways including apoptosis, inflammation, ER stress, and autophagy[59]. The impact of
489 long-chain fatty acid lipotoxicity on *CXCL1* expression is documented in hepatoma cells[60] similar to our
490 findings in colonoids. Hence, it is plausible that approaches that suppress aberrant epithelial lipid
491 accumulation, hydrolysis, and oxidation may improve colon epithelial function in UC.
492
493 Our study also suggests a dysregulation of PPAR-α network in the UC epithelium and colonoids. PPARA is
494 a transcriptional regulator of several genes involved in glucose and lipid homeostasis[46], and, indeed, we
495 observed elevated glucose consumption and neutral lipid accumulation in control colonoids treated with a
496 PPAR-α agonist. PPAR-α activation was also associated with hypermetabolic phenotype, morphologic and
497 molecular evidence of impaired differentiation, similar to our observation in aUC colonoids. Consistent with
498 our study, PPAR-α agonism through fenofibrate exaggerated colitis in DSS-induced mouse models with a
499 concomitant increase in bioactive serum lipids such as sphingomyelins and ceramides[61,62]. Furthermore,
500 activation of fatty acid oxidation partly via PPAR-α promotes intestinal stemness in high-fat diet models[63],
501 suggesting a detrimental effect on intestinal stem cell differentiation and maintenance of epithelial
502 homeostasis. Earlier studies in adult UC showed that natural agonists of PPAR-α such as PUFAs, are
503 disproportionally accumulated in the inflamed colon mucosa of UC patients which correlated positively with
504 endoscopic disease activity[64,65]. Thus, an understanding of PPAR-α-regulated molecules that are specifically
505 dysregulated in pediatric aUC samples may provide specific mechanistic targets for future studies.
506
507 In contrast, pharmacological inhibition of PPAR-α in aUC colonoids blocked aberrant neutral lipid
508 accumulation and thus, suppressed lipid-dependent energy generation during differentiation. PPAR-α
509 inhibition also reduced aUC colonoid hypermetabolism and proton leak. In this scenario, aUC colonoids
510 consumed more glucose likely due to a metabolic switch to compensate for the loss of lipid-dependent
511 oxidation for energy. This lipid-starvation state and the resulting metabolic switch enhanced expression of
512 genes related to differentiation including *WFDC2*. Further, the PPAR-α antagonist reduced cytotoxicity and

513 expression of the chemokine CXCL1, which is critical for neutrophil infiltration in IBD[66]. Hypermetabolism
514 may divert energy expenditure towards translational processes that upregulate cytokine and stress
515 responses[49]; hence, it is plausible that the blockade of lipid's contribution to the hypermetabolic state in aUC
516 colonoids by PPAR-α inhibition reduces such responses. Animal studies have suggested the potential of
517 PPAR-α inhibition in ameliorating colitis induced by epithelial injury[67,68]. Overall, our study in human patient-
518 derived colonoids suggests that PPAR-α antagonism in the epithelium may be a viable treatment strategy
519 for reducing lipotoxicity and hypermetabolic stress in the UC epithelium.
520
521 In conclusion, our data in patient-derived epithelial colon organoids indicate that hypermetabolism and lipid
522 metabolic dysregulation are significant contributors to the epithelial pathogenesis of pediatric UC.
523 Furthermore, epithelial PPAR-α may be a therapeutic target for restoring colon epithelial homeostasis by
524 reducing dysregulated lipid metabolism and normalizing cellular respiration. The use of patient-derived
525 colonoids in this study opens novel research directions in colon epithelial metabolism that may identify
526 metabolic targets for next-generation therapies specifically directed toward healing the colon epithelia in
527 pediatric UC.
528

529 **Methods**

530

531 Human Study Approval and Informed Consent

532

533 Pediatric patient recruitment occurred at Cincinnati Children's Hospital Medical Center, Cincinnati, Ohio,
534 and Lucile Packard Children's Hospital Stanford, Palo Alto, California. Patient data and biopsy collection
535 followed approved protocols by the Research Ethics Committees at each institution. Four to eight colon
536 biopsies (2–5 mm^3) from patients with active UC, inactive UC, and non-IBD controls were collected into ice-
537 cold DMEM/F12 (Corning 10-092-CV) + 50 µg/mL Normocin (InvivoGen #ant-nr) during clinically-indicated
538 lower endoscopy and transported on ice to the lab for immediate processing for spheroid generation.
539 Patient demographics and clinical data are presented in **Supplementary Table 1**.

540

541 Biopsy processing and spheroid culture

542

543 Fresh biopsies were transferred into 5 mL of 2 mM PBS-EDTA and incubated for 45 min on a rotator in a
544 cold room. Biopsies were transferred into 2.5 mL ice-cold sorbitol buffer (2% sorbitol, 1% sucrose, 1% BSA,
545 50 µg/mL Normocin) in a petri dish and crypts were gently scraped off using a college cotton tweezer under
546 a dissecting microscope (Leica S9E). Big tissue pieces were removed with a 20 µL pipette tip and the crypts
547 and buffer were transferred into a 15 mL tube. Crypts were sheared briskly with a 1000 µL pipette (80X total
548 with 1 min interval) and the suspension was made up to 14 mL with ice-cold PBS (Gibco #10010-023). The
549 suspension was centrifuged (300 x g, 5 mins, 4°C) and the pellet was resuspended in organoid wash
550 medium, OWM, (DMEM/F12, 10% FBS, 50 µg/mL Normocin, and washed twice (300 x g, 5 mins, 4°C). The
551 visible pellet was resuspended in growth factor-reduced Matrigel (Corning #356231) and 50 µL drops of the
552 Matrigel mixture were allowed to polymerize at 37°C for at least 15 mins on pre-warmed 12-well plates.
553 Upon stabilization, 700 µL of Intesticult organoid growth medium, OGM, (STEMCELL Technologies,
554 #06010) containing 10 µM TGF-beta receptor inhibitor, SB431542 (Cayman Chemical, #13031), 10 µM
555 ROCK inhibitor, Y27632 (STEMCELL Technologies, #72304), and 50 µg/mL Normocin. Crypts were placed
556 in a tissue culture incubator (37°C, 5% CO2) and OGM was replaced every 2-3 days for the first 7-14 days.

557 Spheroids were considered stable and mature enough for expansion when >70% of spheroids are ~100 μm
558 in diameter.
559
560 For spheroid expansion, OGM was aspirated and 1mL of ice-cold PBS was added to each well. The
561 Matrigel domes were dislodged from the bottom of the plate with a 1000 μL pipette and the PBS-Matrigel
562 mixture was transferred into a 15 mL tube. The Matrigel was broken up inside the tube with a 1000 μL
563 pipette, made up to 5 mL with ice-cold PBS, and incubated on ice for 5 min. The suspension was
564 centrifuged (300 x g, 5 mins, 4°C), 350 uL of TrypLE Express (Gibco #12604-013) was added to the
565 spheroid pellets and incubated in a 37 °C water bath for 4-5 mins. Spheroids were broken up by pipetting
566 50X with a 1000 μL pipette followed by the addition of 5 mL ice-cold OWM. Spheroids were washed twice in
567 OWM (300 x g, 5 mins, 4°C), the resulting pellets were resuspended in 3 parts of Matrigel to 1 part of OWM,
568 and 50 μL drops of the Matrigel suspension were plated in pre-warmed 12-well plates and allowed to
569 polymerize as previously described. For spheroid expansion, 2-3 drops of this suspension were plated per
570 well of a 12-well plate and 800 μL of L-WRN conditioned medium[69,70] was added and replaced every other
571 day.
572
573 For cryopreservation, spheroids underwent at least 3 passages before storage in our pediatric organoid
574 biobank. Matrigel domes with matured spheroids (~80 μm) were dislodged in ice-cold PBS and centrifuged
575 as previously described. Pellets were resuspended in freezing medium (90% FBS, 10% DMSO), and 1 mL
576 of the suspension was added to a cryotube. Samples were slow-frozen in a Mr. Frosty freezing container at
577 -80°C and transferred to liquid N_2 for long-term storage. Overall, the pooling of matured spheroids from two
578 Matrigel domes in one cryotube allows for sufficient post-thaw recovery of spheroids.
579 All experiments used cryopreserved spheroids. Withdrawal of cryotubes from the LN_2 tank followed a quick
580 thaw in a 37°C water bath for ~2mins. Cryotube contents were quickly transferred into pre-warmed 6 mL of
581 OWM and centrifuged (300 x g, 5 mins, 20°C). Spheroid pellets were immediately resuspended in 5 mL
582 OWM, washed once, resuspended in a 3:1 mix of Matrigel and OWM, and plated in 50 μL domes as
583 previously described. Cryopreserved spheroids were passaged at least once before usage for all analyses.
584

585 Spheroids processing and plating for analysis

586

587 After 5-7 days after passaging with TrypLE Express, Matrigel domes with matured spheroids were dislodged
588 with ice-cold PBS as previously described and filtered with a 100 µm strainer (pluriSelect). Filtrates were
589 pelleted and washed once in OWM, manually counted, and replated in domes containing a 1:1 mix of
590 Matrigel and OWM (8-15 spheroids per µL depending on the analysis) and maintained in OGM. For all
591 analyses requiring differentiation into colonoids, replated spheroids were allowed to acclimatize overnight in
592 OGM before switching to Intesticult human organoid differentiation medium, ODM, (STEMCELL
593 Technologies, #100-0214) for the indicated differentiation durations with ODM changed every 2 days. In
594 some experiments, matured spheroids were filtered through a 40 µm strainer (Pluriselect) immediately after
595 passaging and cultured in OGM for 6-7 days before counting, replating, and differentiation when necessary.

596

597 To measure drug-induced responses, 2 µM FCCP (Sigma, #C2920), 50 µM Fenofibrate (Abcam,
598 AB120832), and 1 µM GW6471 (Sigma, #G5045) were added to ODM throughout the differentiation as
599 indicated in figure legends. The solvents served as vehicle controls for respective experiments (DMSO for
600 FCCP, and 100% ethanol for Fenofibrate and GW6471). ODM with drugs were removed and colonoids were
601 processed for analyses.

602

603 Spheroid Diameter and Colonoid Budding

604

605 Spheroids were passaged as previously described and filtered through a 40 µm strainer (Pluriselect).
606 Spheroids were manually counted and 750 spheroids were replated per 50 µL dome in pre-warmed 12-well
607 plates and cultured in OGM for 6 days. Phase contrast images were obtained on the Keyence BZ-X800
608 microscope.

609

610 To assess colonoid budding, matured spheroids were counted, replated in 50 µL Matrigel (15 spheroids/µL),
611 and allowed to acclimatize overnight in OGM. Each well was washed with PBS at room temperature (RT) for
612 3 min before switching to ODM for the indicated number of days. Phase contrast images were obtained on

613 the Keyence BZ-X800 microscope. All measurements of spheroid diameter and enumeration of colonoid
614 budding were performed in a manner blinded to colonoid diagnosis group using the Keyence BZ-X800
615 analyzer. The number of buds on each colonoid was presented relative to the total number of visible
616 colonoids per field.
617
618 Extracellular Flux Analyses
619
620 The XF Seahorse MitoStress Test (Agilent) was used to measure oxygen consumption rates (OCR), at
621 baseline, and after the injection of mitochondrial inhibitors[71]. Each spheroid line was replated in
622 quadruplicates as described previously in 15 µL matrigel domes (8 spheroids/µL) containing a 1:1 mix of
623 Matrigel and OWM into Seahorse XF96 cell culture plates (Agilent #101085-004) and cultured overnight in
624 150 µL OGM. The four edges of the plate served as blank with only a 1:1 mix of Matrigel and OWM. For
625 some experiments, 50 µL of OGM was removed after 24 hrs into an empty 96-well plate and stored at -80°C
626 for later measurements of LDH activity. Where differentiation was needed, spheroids were washed once
627 with PBS on the following day and differentiated in 200 µL ODM into colonoids for the indicated number of
628 days in the figure legends. For some experiments, 50 µL of ODM was removed from all wells after 48 hr into
629 an empty 96-well plate and frozen at -80°C for later measurements of glucose, lactose, and LDH activity.
630
631 On the day of the assay, ODM was removed from colonoids, washed once with 200 µL PBS, and replaced
632 with 150 µL DMEM assay medium (Agilent, #103334-100), pH 7.4 containing 10 mM glucose, 2 mM
633 glutamine, and 1 mM pyruvate (all from Agilent). Plates were incubated in a non-CO_2 incubator for 1 hr and
634 OCR was measured at baseline and after a sequential injection of oligomycin (final concentration, 4µM),
635 FCCP (final concentration, 2 µM), and rotenone/antimycin (final concentration, 100 nM/1 µM) using the
636 XF96^{e} Extracellular Flux assay kits on the XF96^{e} analyzer.
637
638 The Glycostress test (Agilent) was used to measure extracellular acidification rates (ECAR) in colonoids
639 after a 3-day differentiation. On the day of the assay, ODM was replaced with base medium (Agilent
640 #103575-100) lacking glucose, pyruvate, and glutamine and incubated in a non-CO_2 incubator for 1 hr.

641 Baseline ECAR was assessed using the XF96^{e} analyzer (Agilent) followed by sequential injections of
642 glucose, oligomycin, and 2-deoxy glucose at final concentrations of 40 μM, 4 μM, and 500 mM, respectively.
643 Raw data were normalized with DNA content as described below.
644
645 For etomoxir experiments, colonoids were differentiated for 3 days. On the day of the assay, ODM was
646 replaced with assay medium (Agilent #103575) lacking glucose, pyruvate, and glutamine, and incubated in
647 a non-CO_2 incubator for 40 min. Etomoxir (Sigma, #E1905) was prepared in the assay medium, quickly
648 added to designated wells within 5 mins at a final concentration of 44 μM, and returned to the non-CO_2
649 incubator for 15 min. OCR assessment followed as described previously.
650
651 DNA extraction
652
653 For the normalization of colonoid extracellular flux data, DNA normalization protocol was used as previously
654 described with modifications[71]. DNA was extracted using the QIAamp DNA Micro kit (Qiagen #56304).
655 Briefly, the medium was removed from the cell culture plates and 45 μL of ATL lysis buffer was added per
656 well, followed by 5 μL of Protein kinase K. The plate was incubated at 56°C for 1 hr, quadruplicate wells
657 were pooled into 1.5 mL tubes and returned to 56°C incubator for 1 hr. DNA extraction continued according
658 to the manufacturer's instructions. The DNA content of each colonoid line was calculated relative to the
659 blank wells and used to normalize raw data.
660
661 Total ATP measurement
662
663 Spheroids were plated in clear flat bottom 96-well tissue culture plates (Falcon #353075) as described for
664 extracellular flux analyses and differentiated for the indicated number of days. Total ATP levels were
665 assayed with the luminescent ATP detection assay kit (Abcam, ab113849), according to the manufacturer's
666 instructions and luminescence was recorded using the Spectramax id5 plate reader (Molecular Devices).
667 ATP levels were normalized by measuring DNA content in a parallel plate as described for extracellular flux
668 analyses.

669

670 Mitochondrial Superoxide (MitoSOX) Analysis

671

672 Spheroids were plated in black 96-well tissue culture plates with clear bottoms (Corning, #3603) as
673 described for extracellular flux analyses and differentiated for the indicated number of days in the figure
674 legends. Mitochondrial ROS was estimated with the fluorescent probe MitoSOX red (Thermofisher,
675 #M36008). Briefly, a 5 mM MitoSOX stock solution was prepared in DMSO and diluted with HBSS to a
676 working concentration of 3 μM. Colonoids were washed twice with HBSS and the MitoSOX working solution
677 was added to the colonoids and incubated for 30 min (37°C, 5% CO2). The colonoids were washed 3 times
678 with HBSS and MitoSOX fluorescence was measured at 396/610 nm using the Spectramax iD5 plate reader
679 (Molecular Devices). Data were normalized by measuring DNA content as described for extracellular flux
680 analyses.

681

682 Lactate Dehydrogenase (LDH) release

683

684 OGM and ODM stored from Seahorse XF96 cell culture plates as described above were thawed on ice and
685 extracellular LDH activity was measured using the LDH-Glo Cytotoxicity assay (Promega, #J2380).
686 Samples were diluted 40X in ice-cold storage buffer (200mM Tris-HCl (pH 7.3), 10% Glycerol, 1% BSA),
687 and LDH activity was measured according to the manufacturer's instructions. Luminescence was recorded
688 using the Spectramax id5 plate reader (Molecular Devices), and the data was normalized with DNA content
689 from the corresponding Seahorse plate as described previously. LDH release from spheroids and colonoids
690 was estimated relative to blank wells in the Seahorse XF96 cell culture plate.

691

692 Extracellular Glucose and Lactate

693

694 ODM from colonoids stored from Seahorse XF96 cell culture plates as previously described were thawed on
695 ice and extracellular glucose and lactate were measured using the Glucose-Glo (Promega, #J6021) and
696 Lactate-Glo (Promega, #J5021) assays, respectively. Samples were diluted 50X in ice-cold PBS and the

697 measurements continued according to the manufacturer's instructions. Luminescence was recorded using
698 the Spectramax id5 plate reader (Molecular Devices), and the data was normalized with DNA content from
699 the corresponding Seahorse plate as described previously. Glucose consumed or lactate produced were
700 estimated relative to ODM in blank Seahorse XF96 cell culture wells.
701
702 Flow Cytometry
703
704 Mitochondrial mass (mtMass) analyses
705 For mtMass analyses, we labeled the mitochondria in spheroids and colonoids using the MitoTracker Green
706 FM probe (Cell Signaling, #9074). Briefly, single cells from matured spheroids (15 spheroids/μL) and
707 corresponding colonoids were obtained by the addition of 900 μL TrypLE Express followed by incubation at
708 37°C for 10 mins. Single cells were released by vortexing for 20 seconds with 10-second intervals, and
709 washed in FACS buffer (5% FBS in PBS). Pellets were resuspended in 150 nM mtGreen solution prepared
710 in phenol-red free DMEM/F12 + 5% FBS, followed by incubation for 30 mins at 37°C in a 5% CO_2 incubator.
711 Cells were washed twice in 2 mL PBS and resuspended in 500 μL of ice-cold PBS. The cells were passed
712 through Falcon FACS tubes with a cell strainer cap (Fisher, #0877123) and incubated with 5 μL of the live-
713 dead stain, 7-Aminoactinomycin D (7-AAD), for 5 mins on ice. The mean fluorescence intensity (MFI) of
714 mtGreen was measured in 5000 events using the FITC channel and following 7-AAD exclusion (PE-Cy5) on
715 the Agilent NovoCyte Flow Cytometer. Analysis and images were obtained using the FlowJo software v.10.
716
717 Mitochondrial Membrane Potential (MMP)
718 Single cells from colonoids were processed as previously described and MMP was assessed with the
719 MitoProbe JC-1 assay kit (Thermo Fisher Scientific, MP34152) following the manufacturer's protocol.
720 Briefly, Cells were incubated with 1 μM JC-1 in PBS for 30 mins at 37°C, 5% CO_2. The cells were washed
721 once with PBS and passed through Falcon FACS tubes with a cell strainer cap and incubated with 5 μL of
722 7-AAD, for 5 mins on ice. 10000 events from each line were recorded using the Agilent NovoCyte Flow
723 Cytometer. After 7-AAD exclusion, MMP was calculated as the MFI ratio of the red (PE)/green (FITC)
724 channels.

725

726 BODIPY Neutral lipids

727 Matured spheroids from each line were replated (15 spheroids/μL) in two wells of a 24-well plate and
728 allowed to stabilize overnight in OGM. For each line, one well was switched to ODM to initiate differentiation
729 into colonoids for 2 days while the other well continued in OGM. Single cells were processed from spheroids
730 and colonoids from each line as previously described and cell pellets were fixed using the Cytofix/Cytoperm
731 kit (BD Biosciences, #555028) according to the manufacturer's instructions. Neutral lipid droplets in cells
732 were stained with 1μg/mL BODIPY 493/503 (Thermo Fisher Scientific, #D3922) in PBS for 1 hr at RT with
733 gentle mixing every 20 mins. Cells were washed once with 2 mL PBS and passed through Falcon FACS
734 tubes with a cell strainer cap. BODIPY MFI was recorded in 5000 events using the FITC channel on the
735 Agilent NovoCyte Flow Cytometer. Analysis and images were obtained using the FlowJo software v.10.

736

737

738 Immunofluorescence Imaging

739

740 Colonoid Embedding in Optical Cutting Temperature (OCT) compound

741 Matured spheroids from each line were replated (15 spheroids/μL, 3:1 mixture of Matrigel and OWM) as
742 previously described in 6 domes per well of a 6-well plate. After a 3-day differentiation, colonoids were fixed
743 with 5 mL of 2% Paraformaldehyde and 0.1% Glutaraldehyde for 30 mins at RT. Colonoids were washed 3X
744 with 5 mL PBS for 10 min, and each Matrigel dome was carefully scooped into a 50 mL tube with 20%
745 sucrose in PBS. After 2-3 days following the sinking of all domes, 6 domes/line was embedded in Tissue
746 Tek OCT compound (Sakura Finetek, #4583) and frozen in liquid N_2 using the Seal'N Freeze cryotray and
747 box (Fisher Scientific, #NC1877501). From the Colonoid OCT block, 10 μm thick cryosections were cut on
748 slides and stored at -80°C. For immunostaining, cryosections were washed once with PBS for 15 secs at RT
749 followed by autofluorescence quenching by incubation with 10 mM Sodium Borohydride in PBS twice for 5
750 mins at RT. Sections were washed thrice in PBS for 10 minutes each, followed by permeabilization with
751 0.15% Triton X-100 for 15 mins at RT. Slides were washed thrice with PBS and incubated with the blocking
752 buffer (3% BSA, 5% donkey serum, and 5% goat serum in PBS) for 1 hr at RT. This was followed by

753 overnight incubation with primary antibodies rabbit anti-UCP2 (1:100, Proteintech, #11081-1-AP) and
754 mouse anti-COX4 (1:200, Invitrogen, GT6310) in the blocking buffer in a humidified chamber at 4°C. Slides
755 were washed twice with PBS for 15 secs, followed by 2X wash in PBS for 5 mins. Slides were incubated in
756 a humidified chamber for 1 hr at RT in secondary antibodies: donkey anti-rabbit Alexa Flour 647 (1:1000,
757 Invitrogen, #A31573) and goat anti-mouse Alexa Flour 488 (1:1000, Invitrogen, #A11001) prepared in
758 blocking buffer. Slides were washed 3X in PBS and counterstained with Phalloidin (1:250, ThermoFisher
759 Scientific #T7471) in PBS for 30 min at RT. Slides were washed once in distilled water and mounted in
760 Prolong Glass Antifade Mountant with NucBlue Stain containing the Hoechst 33342 DNA marker
761 (ThermoFisher Scientific, #P36983). Images were acquired on the Keyence BZ-X800 microscope. Images
762 were merged with the Keyence BZ-X800 software analyzer and cells expressing DAPI and those co-
763 expressing UCP2 and COX4 were counted on at least four high-power fields (60X oil objective) per patient
764 colonoid line.
765
766 Colonoid whole-mount staining
767 For whole-mount staining, matured spheroids were replated (15 spheroids/µL, 1:1 mixture of Matrigel and
768 OWM) as previously described in 8-well chamber µ-slides (IBIDI, #80826). After differentiation, colonoids
769 were washed with PBS at RT and fixed with 500 µL of 4% PFA for 30 mins at RT. For UCP2 staining,
770 colonoids were washed 2X with 500 µL PBS for 5 mins and permeabilized with 0.2% Triton X-100 in PBS
771 for 30 mins at RT followed by 2X wash in PBS. Samples were incubated with 50 mM ammonium chloride
772 (NH_4Cl) in PBS for 30 mins at RT to quench potential autofluorescence. After a 2X wash in PBS, samples
773 were incubated in blocking buffer (3% BSA, 5% donkey serum in PBS) for 1 hr at RT and incubated in
774 primary antibody- rabbit anti-UCP2 (1:50, Proteintech, #11081-1-AP) overnight and secondary antibody-
775 donkey anti-rabbit Alexa Flour 647 (1:500, Invitrogen, #A31573) for 1 hr at RT, and incubated with Phalloidin
776 as previously described. Samples were mounted in 200 µL Fructose-glycerol clearing solution[72] and
777 incubated for 30 mins at RT. Whole-mount images were acquired using the Stellaris 8 Inverted Confocal
778 Microscope (Leica) using the 20x oil objective and individual channels were merged using the Leica LAS X
779 software.
780

781 For visualizing neutral lipids, colonoids differentiated for 2 days in chamber slides were fixed in 4% PFA,
782 washed, and incubated in 50 mM NH_4Cl as previously described. Then colonoids were stained with 1 µg/mL
783 BODIPY 493/503 (Thermo Fisher Scientific, #D3922) in PBS for 1 hr at RT, washed twice in PBS, and
784 incubated with Phalloidin as previously described. Chamber slides were washed once in distilled water and
785 mounted in 2 drops of Prolong Glass Antifade Mountant with NucBlue Stain containing the Hoechst 33342
786 DNA marker (ThermoFisher Scientific, #P36983). Samples were allowed to cure overnight at RT in the dark.
787 Whole-mount images were acquired using the Stellaris 8 Inverted Confocal Microscope (Leica) as
788 previously described.
789
790 RNA processing and Bulk RNA sequencing
791
792 RNA was processed concurrently from eight patient organoid lines per diagnosis using the RNeasy Micro
793 Kit (Qiagen, #74004). Briefly, matured spheroids from each line (n=8 per diagnosis) were filtered through a
794 100 µm strainer (Pluriselect), replated (15 spheroids/µL, 2:1 mixture of Matrigel and OWM) in two wells of a
795 12-well plate (3 domes/well) and allowed to stabilize overnight in 800 µL OGM. The following day, one well
796 of spheroids/line was processed for RNA extraction, while the other well was switched to ODM for
797 differentiation into colonoids for 3 days. For RNA extraction, the medium was removed, and Matrigel domes
798 were dislodged with PBS from the bottom of the plate as previously described. To digest and remove any
799 traces of Matrigel, the suspension was centrifuged (300 x g, 5 mins, 4°C), 350 µL of TrypLE Express (Gibco)
800 was added to the spheroid pellets and incubated in a 37°C water bath for 3 mins. The tube was swirled
801 briefly followed by the addition of 5 mL ice-cold OWM. Samples were washed (300 x g, 5 mins, 4°C), and
802 the supernatant was aspirated. Any remnants of OWM were carefully removed with a 200 µL pipette and the
803 resulting pellets were resuspended in the lysis buffer from the RNeasy Micro Kit and stored immediately at -
804 80°C. Further processing of RNA followed the manufacturer's instructions. RNA sequencing of poly-A
805 enriched RNA libraries was carried out on the Illumina NovaSeq PE150 platform (Novogene). RNA-seq
806 reads were aligned to the human reference hg38 genome and the nf-core/rnaseq (v3.5) workflow was used
807 for developing the expression matrix.
808

809 Ingenuity Pathway Analysis (IPA)

810

811 Fold changes from the colonoid bulk RNA-seq data (Log2FC and p-adj values) were uploaded into the IPA
812 software and used to predict canonical pathways that underlie transcriptional data. All upregulated and
813 downregulated genes were concurrently analyzed in IPA with an expression p-value cutoff of 0.1. The top
814 biological and cellular pathways and causal networks were selected based on the fisher's exact test p-value
815 which measures the overlap of observed and predicted regulatory gene sets[35].

816

817 Single Cell Data Analyses
818
819
820 We utilized data from the established single-cell transcriptomic atlas of 68 colon biopsies obtained from 18
821 UC patients and 12 healthy controls[39]. Processed single-cell expression matrices and metadata for human
822 colon epithelial cells were obtained from the Single Cell Portal
823 (https://singlecell.broadinstitute.org/single_cell, accession SCP259). Expression counts were normalized
824 using the R (v.4.3.3) package Seurat (v.5.1.0). The reported PPARA, RXR, and lipid-related genes were
825 visualized using the R package ComplexHeatMap (v.2.18.0).

826

827 Quantitative RT PCR

828

829 For most analyses, total RNA was processed from spheroids or colonoids by matrigel removal and digestion
830 as previously described. Due to the short half-life of *UCP2* (ref) samples for *UCP2* analysis were plated in a
831 1:1 mixture of Matrigel and OWM, differentiated, and lysed directly in the culture well without Matrigel
832 removal. For all analyses, RNA was processed (RNeasy Micro Kit, Qiagen, #74004) and cDNA was
833 synthesized using the High-Capacity cDNA Reverse Transcription kit (Applied Biosystems, #4368814).
834 Gene expression was quantified on the QuantStudio 3 thermocycler using Taqman probes (**Supplementary**
835 **Table 5**). Fold changes were quantified using the $2^{-\Delta\Delta CT}$ method using *ACTB* or *GAPDH* as the reference
836 gene where appropriate.

837

838 LPL Activity

839

840 Spheroids were plated, differentiated for 2 days or 5 days, and processed for Matrigel removal as previously
841 described for RNA processing. Total colonoid protein was isolated using the Cell Lytic buffer (Sigma, #2978)
842 with 1X Protease and Phosphatase inhibitor cocktail (ThermoFisher Scientific, #78440). Colonoids were
843 incubated on ice for 30 mins with brief vortexing every 10 mins. Samples were centrifuged (10000 x g, 10
844 mins, 4°C), and the supernatant was transferred into fresh 1.5 mL tubes. Protein concentration was
845 determined using the BCA protein Assay kit (ThermoFisher Scientific, #23227). LPL activity in each sample
846 was determined in duplicates using the LPL activity assay kit (Cell Biolabs, #STA-610) following the
847 manufacturer's instructions, and the data was normalized to total protein concentration.

848

849 Nuclear PPAR-α activity assay

850

851 Three spheroids per group were differentiated in ODM for 24 hrs, pooled, and processed for Matrigel
852 removal as previously described for RNA processing. Nuclei isolation followed the established Omni-ATAC
853 protocol used for nuclei preparations for ATAC-seq[73]. Nuclei protein concentration was determined using the
854 BCA protein Assay kit (ThermoFisher Scientific, #23227). PPAR-α activity was assessed in the nuclear
855 extracts with the PPAR-α activity kit (Abcam, #ab133107) following the manufacturer's instructions.

856

857 Extracellular Chemokine assay

858

859 Spheroids were plated and differentiated in ODM for the indicated days in the figure legend, as previously
860 described for RNA processing. ODM was collected at the indicated days and frozen at -80°C until analyses.
861 For analyses involving differentiation until day 5, ODM was changed on day 2 before collection and
862 analyses on day 5. The total colonoid protein was determined using the Cell Lytic buffer with 1X Protease
863 and Phosphatase inhibitor as previously described. Extracellular chemokines in ODM on the indicated days
864 were assessed using the following kits (CXCL1: Abcam #ab190805, CXCL11: ThermoFisher #EHCXCL11,
865 CCL2: ThermoFisher #88-7399-22, CCL28: ThermoFisher #EHENC1) following manufacturer's instructions.

866

867 BSA-PA assay

868

869 Palmitic acid (PA) complexed to bovine serum albumin (BSA) was prepared based on a previously
870 described protocol with few modifications[60]. Briefly, 50 mg/mL of PA (Sigma, #P0500) was dissolved in
871 100% ethanol (150 x g, 20 mins, 37°C) to make a 195 mM PA stock solution. A 3 mM PA solution was
872 prepared in 10% fat-free BSA (Sigma, #A8806) in PBS and incubated at 47°C for 20 mins on a shaker. For
873 controls, an equivalent amount of EtOH was added to 10% fat-free BSA and processed as previously
874 described for PA. The BSA-PA and BSA-EtOH solutions were distributed into aliquots and stored at -20°C.
875 For colonoid exposure experiments, the solutions were diluted in ODM to prepare the desired
876 concentrations as described in figures and legends.

877

878 Statistical analyses

879 For all data, statistical analysis was conducted in Prism (v.10.0). Due to the varied statistical approaches
880 used in this study, statistical methods for each figure are outlined in individual figure legends. For this study,
881 eight patient-derived colonoids were generated per diagnosis (control, active UC, inactive UC). Wherever
882 representative colonoids were used, the number of independent colonoids and technical replicates used
883 were described in the relevant figure legend or method section. For differentially expressed genes from the
884 RNA-seq data, transcripts with $Log_2FC \geq \pm 1$, FDR $P \leq 0.1$ were considered statistically significant. For all
885 other data *P* values less than 0.05 were considered statistically significant.

886

887 **Data Availability**

888 Bulk RNAseq data sets from spheroids and colonoids in this study were deposited into Gene Expression
889 Omnibus (GEO) under the accession number GSE… . Other appropriate data will be provided by the
890 corresponding author upon request.

891

892

893 **References**

894 1. Reinink, A. R., Lee, T. C. & Higgins, P. D. R. Endoscopic Mucosal Healing Predicts Favorable Clinical
895 Outcomes in Inflammatory Bowel Disease: A Meta-analysis. *Inflamm. Bowel Dis.* **22**, 1859–1869 (2016).
896 2. Colombel, J. F. *et al.* Early mucosal healing with infliximab is associated with improved long-term clinical
897 outcomes in ulcerative colitis. *Gastroenterology* **141**, 1194–1201 (2011).
898 3. Hyams, J. S. *et al.* Clinical and biological predictors of response to standardised paediatric colitis
899 therapy (PROTECT): a multicentre inception cohort study. *The Lancet* **393**, 1708–1720 (2019).
900 4. Danese, S. *et al.* Upadacitinib as induction and maintenance therapy for moderately to severely active
901 ulcerative colitis: results from three phase 3, multicentre, double-blind, randomised trials. *The Lancet*
902 **399**, 2113–2128 (2022).
903 5. Sandborn William J. *et al.* Tofacitinib as Induction and Maintenance Therapy for Ulcerative Colitis. *N.*
904 *Engl. J. Med.* **376**, 1723–1736 (2017).
905 6. Sands, B. E. *et al.* Ustekinumab as Induction and Maintenance Therapy for Ulcerative Colitis. *N. Engl. J.*
906 *Med.* **381**, 1201–1214 (2019).
907 7. Rosen, M. J., Dhawan, A. & Saeed, S. A. Inflammatory Bowel Disease in Children and Adolescents.
908 *JAMA Pediatr.* **169**, 1053–1060 (2015).
909 8. Ye, Y., Manne, S., Treem, W. R. & Bennett, D. Prevalence of Inflammatory Bowel Disease in Pediatric
910 and Adult Populations: Recent Estimates From Large National Databases in the United States, 2007–
911 2016. *Inflamm. Bowel Dis.* **26**, 619–625 (2020).
912 9. Kappelman, M. D., Moore, K. R., Allen, J. K. & Cook, S. F. Recent trends in the prevalence of Crohn's
913 disease and ulcerative colitis in a commercially insured US population. *Dig. Dis. Sci.* **58**, 519–525
914 (2013).
915 10. Kappelman, M. D. *et al.* Direct Health Care Costs of Crohn's Disease and Ulcerative Colitis in US
916 Children and Adults. *Gastroenterology* **135**, 1907–1913 (2008).

917 11. Ardizzone, S. *et al.* Mucosal healing predicts late outcomes after the first course of corticosteroids for
918 newly diagnosed ulcerative colitis. *Clin. Gastroenterol. Hepatol. Off. Clin. Pract. J. Am. Gastroenterol.*
919 *Assoc.* **9**, 483-489.e3 (2011).
920 12. Rogler, G., Vavricka, S., Schoepfer, A. & Lakatos, P. L. Mucosal healing and deep remission: what does
921 it mean? *World J. Gastroenterol.* **19**, 7552–7560 (2013).
922 13. Neurath, M. F. & Travis, S. P. L. Mucosal healing in inflammatory bowel diseases: a systematic review.
923 *Gut* **61**, 1619–1635 (2012).
924 14. Adolph, T. E. *et al.* The metabolic nature of inflammatory bowel diseases. *Nat. Rev. Gastroenterol.*
925 *Hepatol.* **19**, 753–767 (2022).
926 15. Aldars-García, L., Gisbert, J. P. & Chaparro, M. Metabolomics Insights into Inflammatory Bowel
927 Disease: A Comprehensive Review. *Pharm. Basel Switz.* **14**, 1190 (2021).
928 16. Fu, S.-C. *et al.* Excessive Mitochondrial Fission Suppresses Mucosal Repair by Impairing Butyrate
929 Metabolism in Colonocytes. *Inflamm. Bowel Dis.* **30**, 114–124 (2024).
930 17. Sifroni, K. G. *et al.* Mitochondrial respiratory chain in the colonic mucosal of patients with ulcerative
931 colitis. *Mol. Cell. Biochem.* **342**, 111–115 (2010).
932 18. Santhanam, S. *et al.* Mitochondrial Electron Transport Chain Complex Dysfunction in the Colonic
933 Mucosa in Ulcerative Colitis. *Inflamm. Bowel Dis.* **18**, 2158–2168 (2012).
934 19. Haberman, Y. *et al.* Ulcerative colitis mucosal transcriptomes reveal mitochondriopathy and
935 personalized mechanisms underlying disease severity and treatment response. *Nat. Commun.* **10**, 38
936 (2019).
937 20. Novak, E. A. & Mollen, K. P. Mitochondrial dysfunction in inflammatory bowel disease. *Front. Cell Dev.*
938 *Biol.* **3**, (2015).
939 21. Clevers, H. Modeling Development and Disease with Organoids. *Cell* **165**, 1586–1597 (2016).
940 22. Ojo, B. A., VanDussen, K. L. & Rosen, M. J. The Promise of Patient-Derived Colon Organoids to Model
941 Ulcerative Colitis. *Inflamm. Bowel Dis.* **28**, 299–308 (2022).

942 23. Dotti, I. *et al.* Alterations in the epithelial stem cell compartment could contribute to permanent changes
943 in the mucosa of patients with ulcerative colitis. *Gut* **66**, 2069–2079 (2017).
944 24. Sarvestani, S. K. *et al.* Cancer-predicting transcriptomic and epigenetic signatures revealed for
945 ulcerative colitis in patient-derived epithelial organoids. *Oncotarget* **9**, 28717–28730 (2018).
946 25. Arnauts, K. *et al.* Ex Vivo Mimicking of Inflammation in Organoids Derived From Patients With
947 Ulcerative Colitis. *Gastroenterology* **159**, 1564–1567 (2020).
948 26. Nanki, K. *et al.* Somatic inflammatory gene mutations in human ulcerative colitis epithelium. *Nature* **577**,
949 254–259 (2020).
950 27. Howell, K. J. *et al.* DNA Methylation and Transcription Patterns in Intestinal Epithelial Cells From
951 Pediatric Patients With Inflammatory Bowel Diseases Differentiate Disease Subtypes and Associate
952 With Outcome. *Gastroenterology* **154**, 585–598 (2018).
953 28. Beumer, J. & Clevers, H. Hallmarks of stemness in mammalian tissues. *Cell Stem Cell* **31**, 7–24 (2024).
954 29. Parikh, K. *et al.* Colonic epithelial cell diversity in health and inflammatory bowel disease. *Nature* **567**,
955 49–55 (2019).
956 30. Burclaff, J. *et al.* A Proximal-to-Distal Survey of Healthy Adult Human Small Intestine and Colon
957 Epithelium by Single-Cell Transcriptomics. *Cell. Mol. Gastroenterol. Hepatol.* **13**, 1554–1589 (2022).
958 31. Nicholls, D. G. Mitochondrial proton leaks and uncoupling proteins. *Biochim. Biophys. Acta BBA -*
959 *Bioenerg.* **1862**, 148428 (2021).
960 32. Pelia, R. *et al.* Profiling non-coding RNA levels with clinical classifiers in pediatric Crohn's disease. *BMC*
961 *Med. Genomics* **14**, 194 (2021).
962 33. van Heel, D. A. *et al.* Inflammatory bowel disease susceptibility loci defined by genome scan meta-
963 analysis of 1952 affected relative pairs. *Hum. Mol. Genet.* **13**, 763–770 (2004).
964 34. Garrity-Park, M. M., Loftus, E. V., Sandborn, W. J., Bryant, S. C. & Smyrk, T. C. MHC Class II alleles in
965 ulcerative colitis-associated colorectal cancer. *Gut* **58**, 1226–1233 (2009).
966 35. Krämer, A., Green, J., Pollard, J. & Tugendreich, S. Causal analysis approaches in Ingenuity Pathway
967 Analysis. *Bioinforma. Oxf. Engl.* **30**, 523–530 (2014).

968 36. TeSlaa, T. & Teitell, M. A. Techniques to monitor glycolysis. *Methods Enzymol.* **542**, 91–114 (2014).
969 37. Althaher, A. R. & Alwahsh, M. An overview of ATP synthase, inhibitors, and their toxicity. *Heliyon* **9**,
970 e22459 (2023).
971 38. Benatzy, Y., Palmer, M. A. & Brüne, B. Arachidonate 15-lipoxygenase type B: Regulation, function, and
972 its role in pathophysiology. *Front. Pharmacol.* **13**, 1042420 (2022).
973 39. Smillie, C. S. *et al.* Intra- and Inter-cellular Rewiring of the Human Colon during Ulcerative Colitis. *Cell*
974 **178**, 714-730.e22 (2019).
975 40. Umar, S. Intestinal Stem Cells. *Curr. Gastroenterol. Rep.* **12**, 340–348 (2010).
976 41. Beyaz, S. *et al.* High fat diet enhances stemness and tumorigenicity of intestinal progenitors. *Nature*
977 **531**, 53–58 (2016).
978 42. Fala, A. M. *et al.* Unsaturated fatty acids as high-affinity ligands of the C-terminal Per-ARNT-Sim
979 domain from the Hypoxia-inducible factor 3α. *Sci. Rep.* **5**, 12698 (2015).
980 43. Soltoff, S. P. Evidence that tyrphostins AG10 and AG18 are mitochondrial uncouplers that alter
981 phosphorylation-dependent cell signaling. *J. Biol. Chem.* **279**, 10910–10918 (2004).
982 44. Abdul-Wahed, A., Guilmeau, S. & Postic, C. Sweet Sixteenth for ChREBP: Established Roles and
983 Future Goals. *Cell Metab.* **26**, 324–341 (2017).
984 45. Liu, Y. *et al.* Bif-1 deficiency impairs lipid homeostasis and causes obesity accompanied by insulin
985 resistance. *Sci. Rep.* **6**, 20453 (2016).
986 46. Bougarne, N. *et al.* Molecular Actions of PPARα in Lipid Metabolism and Inflammation. *Endocr. Rev.* **39**,
987 760–802 (2018).
988 47. Konjar, Š., Pavšič, M. & Veldhoen, M. Regulation of Oxygen Homeostasis at the Intestinal Epithelial
989 Barrier Site. *Int. J. Mol. Sci.* **22**, 9170 (2021).
990 48. Mas-Bargues, C. *et al.* Relevance of Oxygen Concentration in Stem Cell Culture for Regenerative
991 Medicine. *Int. J. Mol. Sci.* **20**, 1195 (2019).
992 49. Sturm, G. *et al.* OxPhos defects cause hypermetabolism and reduce lifespan in cells and in patients
993 with mitochondrial diseases. *Commun. Biol.* **6**, 1–22 (2023).

994 50. Sercel, A. J. *et al.* Hypermetabolism and energetic constraints in mitochondrial disorders. *Nat. Metab.* **6**,
995 192–195 (2024).
996 51. Picard, M. & Turnbull, D. M. Linking the metabolic state and mitochondrial DNA in chronic disease,
997 health, and aging. *Diabetes* **62**, 672–678 (2013).
998 52. Maassen, J. A., Romijn, J. A. & Heine, R. J. Fatty acid-induced mitochondrial uncoupling in adipocytes
999 as a key protective factor against insulin resistance and beta cell dysfunction: a new concept in the
1000 pathogenesis of obesity-associated type 2 diabetes mellitus. *Diabetologia* **50**, 2036–2041 (2007).
1001 53. Lan, A. *et al.* Mitochondrial remodeling and energy metabolism adaptations in colonic crypts during
1002 spontaneous epithelial repair after colitis induction in mice. *Free Radic. Biol. Med.* **205**, 224–233 (2023).
1003 54. Boldyreva, L. V., Morozova, M. V., Saydakova, S. S. & Kozhevnikova, E. N. Fat of the Gut: Epithelial
1004 Phospholipids in Inflammatory Bowel Diseases. *Int. J. Mol. Sci.* **22**, 11682 (2021).
1005 55. Hua, X. *et al.* Inflammatory Bowel Disease Is Associated With Prediagnostic Perturbances in Metabolic
1006 Pathways. *Gastroenterology* **164**, 147-150.e2 (2023).
1007 56. Mourad, F. H., Barada, K. A. & Saade, N. E. Impairment of Small Intestinal Function in Ulcerative
1008 Colitis: Role of Enteric Innervation. *J. Crohns Colitis* **11**, 369–377 (2017).
1009 57. Hamabata, T., Nakamura, T., Masuko, S., Maeda, S. & Murata, T. Production of lipid mediators across
1010 different disease stages of dextran sodium sulfate-induced colitis in mice. *J. Lipid Res.* **59**, 586–595
1011 (2018).
1012 58. Jarc, E. & Petan, T. Lipid Droplets and the Management of Cellular Stress. *Yale J. Biol. Med.* **92**, 435–
1013 452 (2019).
1014 59. Lipke, K., Kubis-Kubiak, A. & Piwowar, A. Molecular Mechanism of Lipotoxicity as an Interesting Aspect
1015 in the Development of Pathological States-Current View of Knowledge. *Cells* **11**, 844 (2022).
1016 60. Dahlquist, K. J. V., Voth, L. C., Fee, A. J. & Stoeckman, A. K. An Autocrine Role for CXCL1 in
1017 Progression of Hepatocellular Carcinoma. *Anticancer Res.* **40**, 6075–6081 (2020).
1018 61. Qi, Y. *et al.* PPARα-dependent exacerbation of experimental colitis by the hypolipidemic drug
1019 fenofibrate. *Am. J. Physiol. Gastrointest. Liver Physiol.* **307**, G564-573 (2014).

1020 62. Gu, X. *et al.* GC-MS metabolomics on PPARα-dependent exacerbation of colitis. *Mol. Biosyst.* **11**,
1021 1329–1337 (2015).
1022 63. Mana, M. D. *et al.* High-fat diet-activated fatty acid oxidation mediates intestinal stemness and
1023 tumorigenicity. *Cell Rep.* **35**, 109212 (2021).
1024 64. Nishida, T. *et al.* Increased arachidonic acid composition of phospholipids in colonic mucosa from
1025 patients with active ulcerative colitis. *Gut* **28**, 1002–1007 (1987).
1026 65. Pearl, D. S. *et al.* Altered colonic mucosal availability of n-3 and n-6 polyunsaturated fatty acids in
1027 ulcerative colitis and the relationship to disease activity. *J. Crohns Colitis* **8**, 70–79 (2014).
1028 66. Huo, A. & Wang, F. Biomarkers of ulcerative colitis disease activity CXCL1, CYP2R1, LPCAT1, and
1029 NEU4 and their relationship to immune infiltrates. *Sci. Rep.* **13**, 12126 (2023).
1030 67. Wang, L. *et al.* rSj16 Protects against DSS-Induced Colitis by Inhibiting the PPAR-α Signaling Pathway.
1031 *Theranostics* **7**, 3446–3460 (2017).
1032 68. Yao, H. *et al.* Matrine protects against DSS-induced murine colitis by improving gut barrier integrity,
1033 inhibiting the PPAR-α signaling pathway, and modulating gut microbiota. *Int. Immunopharmacol.* **100**,
1034 108091 (2021).
1035 69. Miyoshi, H. & Stappenbeck, T. S. In vitro expansion and genetic modification of gastrointestinal stem
1036 cells in spheroid culture. *Nat. Protoc.* **8**, 2471–2482 (2013).
1037 70. VanDussen, K. L., Sonnek, N. M. & Stappenbeck, T. S. L-WRN conditioned medium for gastrointestinal
1038 epithelial stem cell culture shows replicable batch-to-batch activity levels across multiple research
1039 teams. *Stem Cell Res.* **37**, 101430 (2019).
1040 71. Ludikhuize, M. C., Meerlo, M., Burgering, B. M. T. & Rodríguez Colman, M. J. Protocol to profile the
1041 bioenergetics of organoids using Seahorse. *STAR Protoc.* **2**, 100386 (2021).
1042 72. Dekkers, J. F. *et al.* High-resolution 3D imaging of fixed and cleared organoids. *Nat. Protoc.* **14**, 1756–
1043 1771 (2019).
1044 73. Corces, M. R. *et al.* An improved ATAC-seq protocol reduces background and enables interrogation of
1045 frozen tissues. *Nat. Methods* **14**, 959–962 (2017).

1046

1047 **Acknowledgments**

1048 This work was funded by the National Institutes of Health (NIH) to M.J.R. under the award number
1049 R21DK123691 and the Stanford Medicine Children's Health Center for IBD and Celiac Disease. B.A.O was
1050 supported by a fellowship from the Stanford Medicine Children's Health Center for IBD and Celiac. This
1051 work utilized computing resources provided by the Stanford Genetics Bioinformatics Service Center. V.DJ.P
1052 was supported by R01HL139664, R01HL160018, R01 HL134776, R01HL59886, 1R01HL172449-01 from
1053 the NIH. S.D was supported by the R01DKDK099222 award from the NIH. We thank L. Prince (Pediatric
1054 Neonatology, Stanford Medicine) for resources for flow cytometry and confocal microscopy. We
1055 acknowledge the support of the National Center for Advancing Translational Sciences of the NIH under
1056 Award Number UL1TR003142. The content is solely the authors' response and does not necessarily
1057 represent the views of the funding agencies.

1058

1059 **Competing interests**

1060 The authors have no competing interests to disclose.

1061

1062 **Author contributions**

1063

1064

Figures

Fig. 1

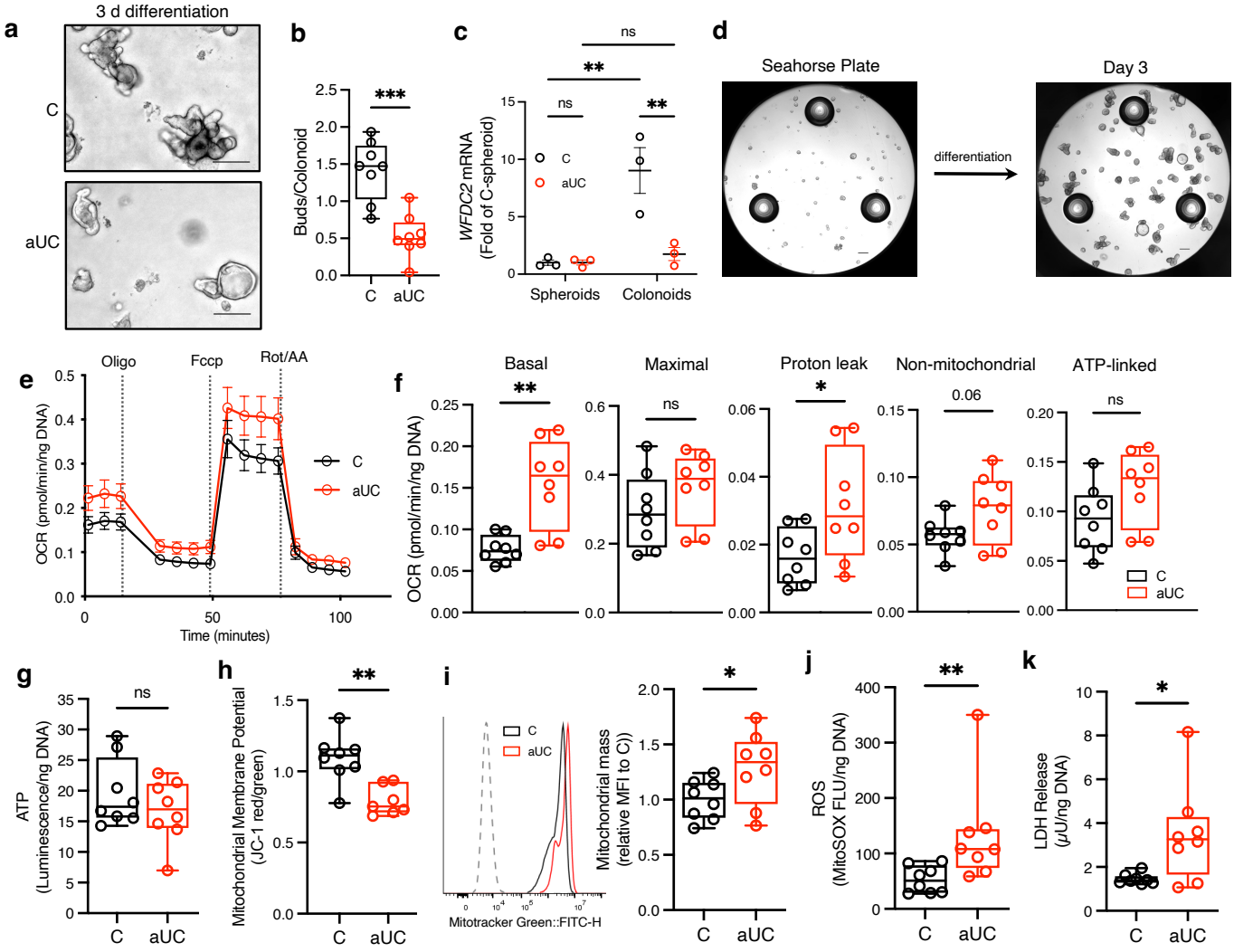

Fig. 1: Hypermetabolism and cellular stress in active UC colonoids during differentiation

a, Representative phase contrast images of pediatric control (C) and active (a)UC colonoids after 3-day differentiation in unstimulated conditions in ODM. Scale bar, 200 μm. **b**, The number of buds/colonoid in colonoids treated as in **a**. Circles represent the average measures of 20-30 colonoids from individual colonoid line**.** n=8 patient colonoid line/group, two-sided Mann-Whitney test. **c**, Spheroids were cultured in OGM, and paired samples were differentiated in ODM for 3 days (colonoids) and assayed for *WFDC2* mRNA abundance using qRT-PCR. n=3 patient line/group, 2-way ANOVA, Fisher LSD test. **d**, Phase

1075 contrast image of a Seahorse 96-well plate with a representative spheroid line before and after 3-day
1076 differentiation. Scale bar, 200 μm **e**, Bioenergetic profile of C and aUC colonoids differentiated for 3 days as
1077 in **a**, and subjected to the Seahorse MitoStress test. Lines represent average measures of individual
1078 colonoid lines. n=8 patient colonoid line/group. **f**, MitoStress OCR response of C and aUC colonoids
1079 differentiated for 3 days as in **a**, in 96-well Seahorse plate. Circles represent the average quadruplicate
1080 wells of individual colonoid lines. n=8 patient colonoid lines/group, Mann-Whitney test. **g**, The colonoids
1081 cultured and used in **f**, were subjected to total ATP luminescence assay. Circles represent the average
1082 luminescence of duplicate wells of individual colonoid lines**.** n=8 patient colonoid line/group, two-sided
1083 Mann-Whitney test. **h**, Colonoids were treated as in **a**, and mitochondrial membrane potential (MMP) was
1084 estimated with the JC-1 dye by flow cytometry. Circles represent the average luminescence of duplicate
1085 wells of individual colonoid lines**.** n=7-8 patient colonoid line/group, two-sided Mann-Whitney test. **i**,
1086 Estimation of mitochondrial mass with Mitotracker green intensity in C and aUC colonoids treated as in **a**.
1087 Circles represent the mean fluorescence intensities (MFI) of 5000 cells from individual colonoid lines. n=8
1088 patient spheroid line/group, two-sided Mann-Whitney test. **j**, The same set of colonoids cultured and used in
1089 **f**, were used to estimate mitochondrial ROS with the MitoSOX fluorescence assay. Circles represent the
1090 average fluorescence of duplicate wells of individual colonoid lines**.** n=8 patient colonoid line/group, two-
1091 sided Mann-Whitney test. **k**, LDH activity in C and aUC colonoids in ODM taken from the same plate as **f**
1092 after a 2-day differentiation. Circles represent the average duplicate measures of individual spheroid lines.
1093 n=8 patient spheroid line/group, unpaired, two-sided t-test. *=$P < 0.05$, **=$P < 0.01$, ***=$P < 0.001$. LDH,
1094 lactate dehydrogenase; OCR, oxygen consumption rates; ODM, organoid differentiation medium; OGM,
1095 organoid growth medium; ROS, reactive oxygen species
1096
1097

Fig. 2:

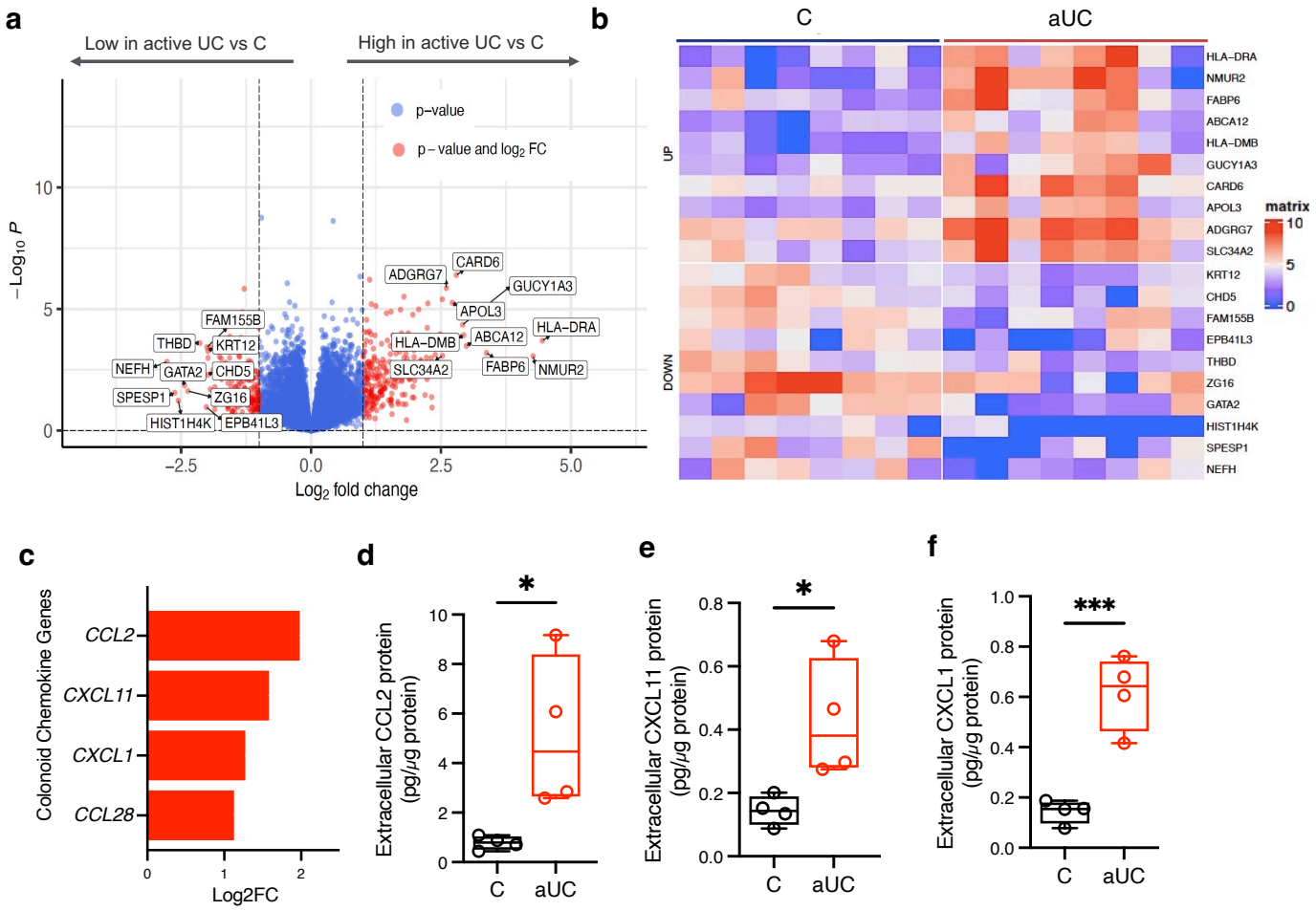

Fig. 2: Distinct transcriptome in epithelial colonoids from active UC pediatric patients

C and aUC pediatric epithelial colonoids differentiated for 3 days in ODM and were subjected to bulk RNA-seq. **a**, Volcano plot of differentially expressed genes between aUC and C samples (Log2FC>1, FDR <0.1). The top 10 dysregulated genes are labeled on the plot. **b,** Heat map of the top 10 dysregulated genes showing the diversity and consistency of expression among each colonoid line n=8 patient colonoid line/group. **c**, Chemokine genes overexpressed in aUC epithelial colonoids compared to C in the bulk RNA-seq data (Log2FC>1, FDR <0.1), n=8 patient colonoid line/group. The full list of differentially expressed genes is provided in Supplementary Table 2. **d**, Robust overexpression of chemokine protein, CCL2, **e**, CXCL11, and **f**, CXCL1 in aUC colonoids using ODM collected after a 3-day differentiation. **d-f**, n=4 patient colonoid lines/group. Circles represent the average of duplicate measures of individual colonoid lines, two-sided unpaired t-test, *=$P < 0.05$, **=$P < 0.01$, ***=$P < 0.001$. ODM, organoid differentiation medium

Fig. 3

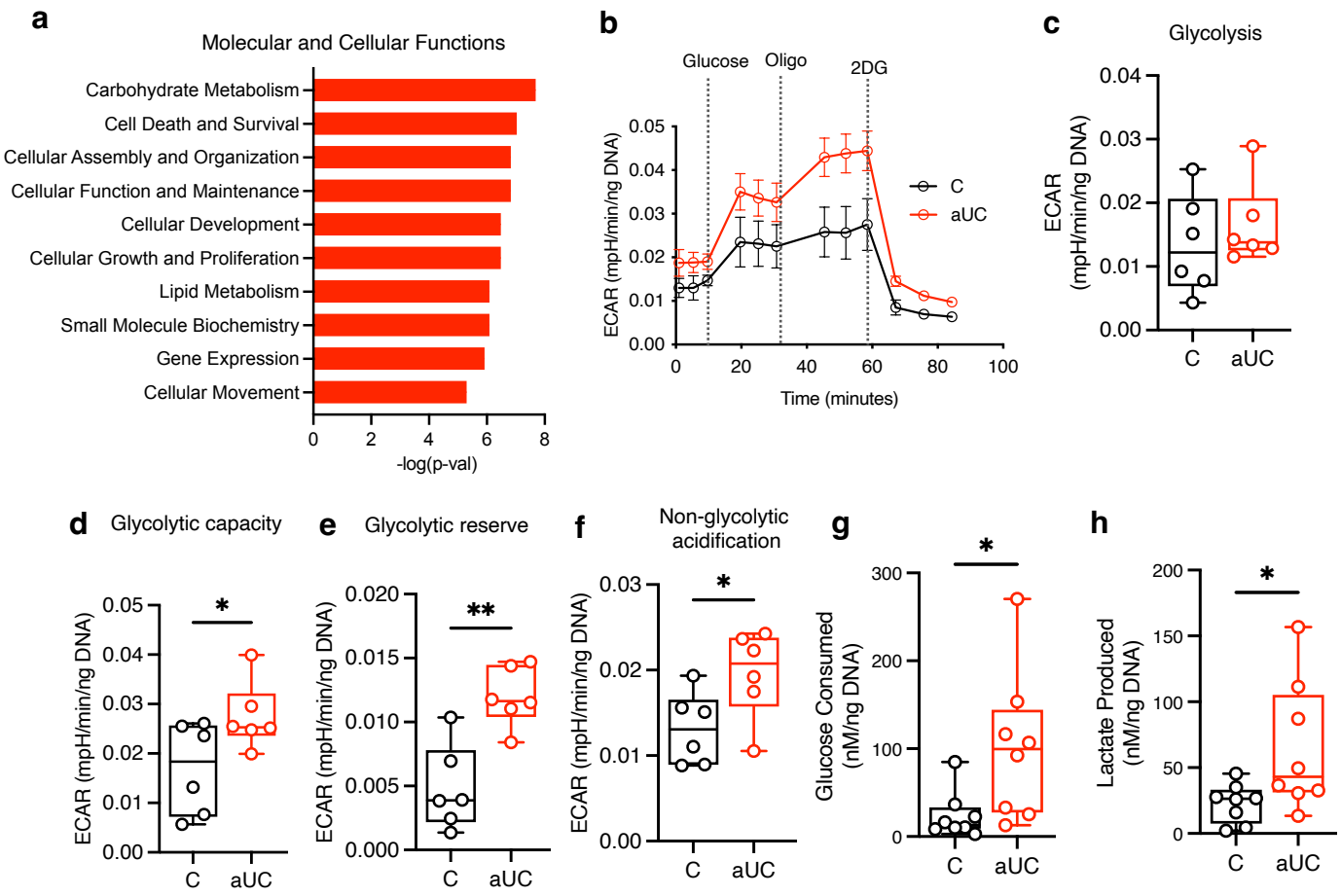

Fig. 3: Higher glycolytic capacity in active UC colonoids during differentiation

a, Ingenuity Pathway Analysis of differentially expressed RNAs between aUC and C colonoids. The top 10 Molecular and Cellular Functions are shown. Full details of molecules involved under each function are presented in Supplementary Table 3. **b**, Bioenergetic profile of C and aUC colonoids differentiated in 96-well Seahorse plates for 3 days under non-stimulated conditions in ODM and subjected to the Seahorse Glycostress assay. Lines represent the average of quadruplicate ECAR measurements from individual colonoid lines. n=6 patient colonoid line/group. **c-f**, Glycostress extracellular acidification rates (ECAR) of C and aUC colonoids as in **b**, to determine real-time **c**, glycolysis, **d**, glycolytic capacity, **e**, glycolytic reserve, and **f**, non-glycolytic acidification rate. Circles in **c-f** represent the average quadruplicate wells of individual colonoid lines. n=6 patient colonoid lines/group, two-sided unpaired t-test. **g**, Extracellular glucose and **h**,

extracellular lactate concentration in 2-day ODM from C and aUC colonoids differentiated for two days. Circles represent the average duplicate measures of individual colonoid lines relative to measures in blank wells with ODM only. n=8 patient colonoid line/group, unpaired, two-sided t-test. *=$P < 0.05$, **=$P < 0.01$. ECAR, extracellular acidification rates, ODM, organoid differentiation medium.

Fig. 4

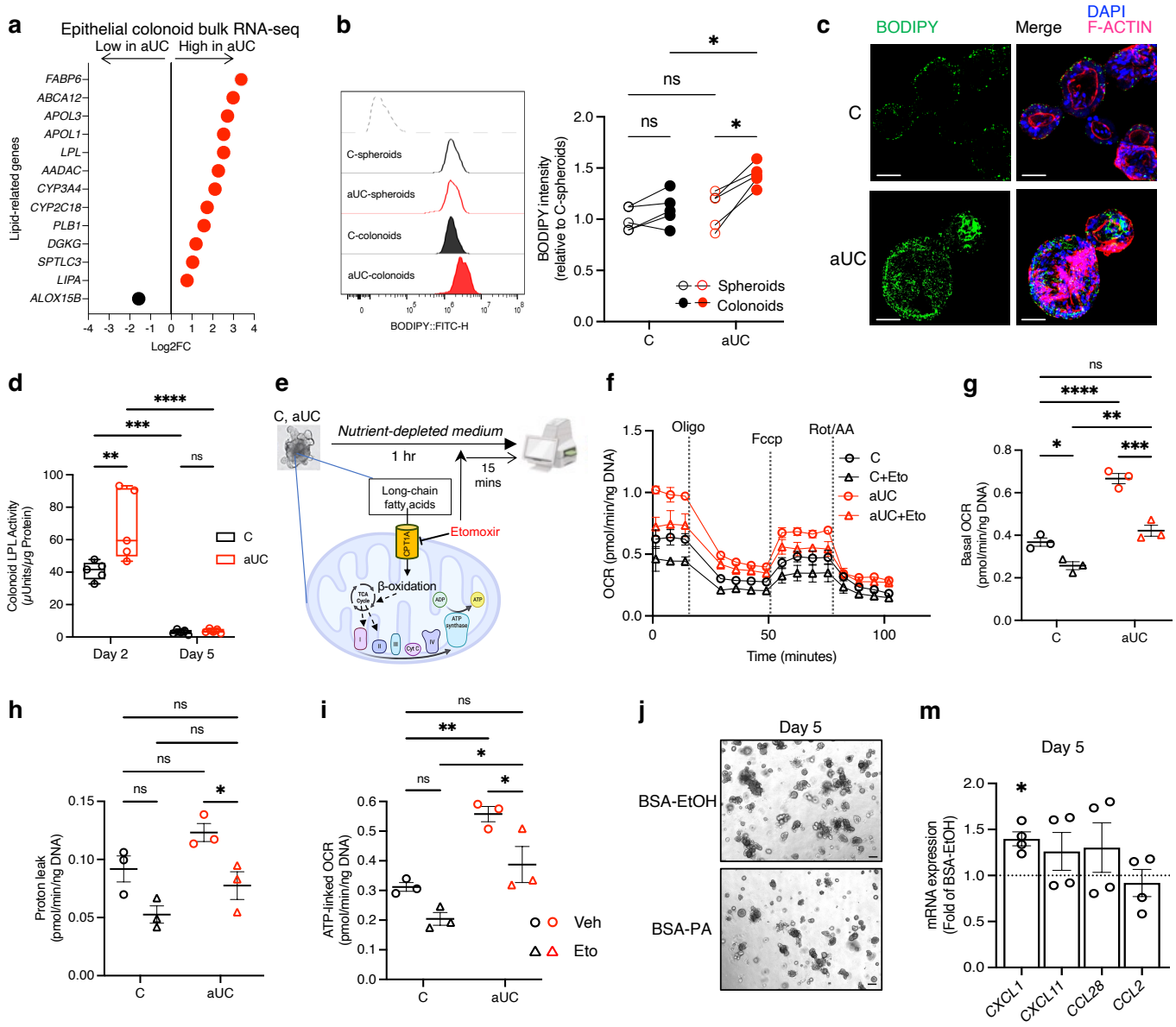

1129 **Fig. 4: Dysregulated lipid metabolism supports hypermetabolism in active UC colonoids during**
1130 **differentiation**

1131 **a**, Significant differentially expressed lipid-related genes (FDR<0.1) in aUC vs C epithelial colonoids
1132 differentiated for 3 days. Dots represent the Log2 fold change in aUC compared to C colonoids. n=8 patient
1133 colonoid lines/group. **b**, Spheroids were cultured in OGM, and paired samples were differentiated in ODM
1134 for 2 days (colonoids) and assayed for BODIPY$^+$ neutral lipid estimation by flow cytometry. Open symbols
1135 represent the mean fluorescence intensities of BODIPY$^+$ cells from individual patient spheroids, while closed
1136 symbols represent the mean fluorescence intensities of BODIPY$^+$ cells from individual colonoid lines. Data
1137 presented relative to C-spheroids. n=5 patient lines/group, 2-way ANOVA, Tukey's *post hoc* test. **c**,
1138 Representative confocal microscopy images of C and aUC colonoids treated as in **b**, for visualizing
1139 BODIPY$^+$ neutral lipid accumulation. Scale bar, 50 μm . **d**, LPL protein activity in C and aUC colonoids after
1140 a 2-day and 5-day differentiation in ODM. Black and Red circles represent the average duplicate measures
1141 of individual colonoid lines. n=5 patient colonoid lines/group. Two-way ANOVA, Fisher's LSD test. **e**,
1142 Schematic of C and aUC colonoids differentiated for 3 days in ODM subjected to the Seahorse MitoStress
1143 test in a nutrient-deprived medium with or without etomoxir to inhibit fatty acid oxidation. **f**, Bioenergetic
1144 profile of C and aUC colonoids as in **e**. Lines represent the average of quadruplicate OCR measures from
1145 individual colonoid lines. n=3 patient colonoid lines/group. **g**, Basal OCR, **h**, proton leak, and **i**, ATP-linked
1146 OCR response of C and aUC colonoids as in **e.** Symbols represent the average triplicate wells of individual
1147 colonoid lines. n=3 patient colonoid lines/group. 2-way ANOVA, Tukey's *post hoc* test. **j**, Representative
1148 phase contrast images of colonoids exposed to 200 μM BSA-PA or BSA-EtOH control for the first 3 days
1149 before further differentiation up to 5 days. Scale bar, 200 μm. **m**, Gene expression of chemokines in
1150 colonoids treated as in **j**, assessed by qRT-PCR. Circles represent individual colonoid lines treated with
1151 BSA-PA relative to those treated with BSA-EtOH**.** n=4 patient colonoid lines/group. Two-sided paired t-test.
1152 *=$P < 0.05$, **=$P < 0.01$, ***=$P < 0.001$. ****=$P < 0.0001$ BSA, bovine serum albumin; OCR, oxygen
1153 consumption rates; ODM, organoid differentiation medium; PA, Palmitic acid
1154

Fig. 5

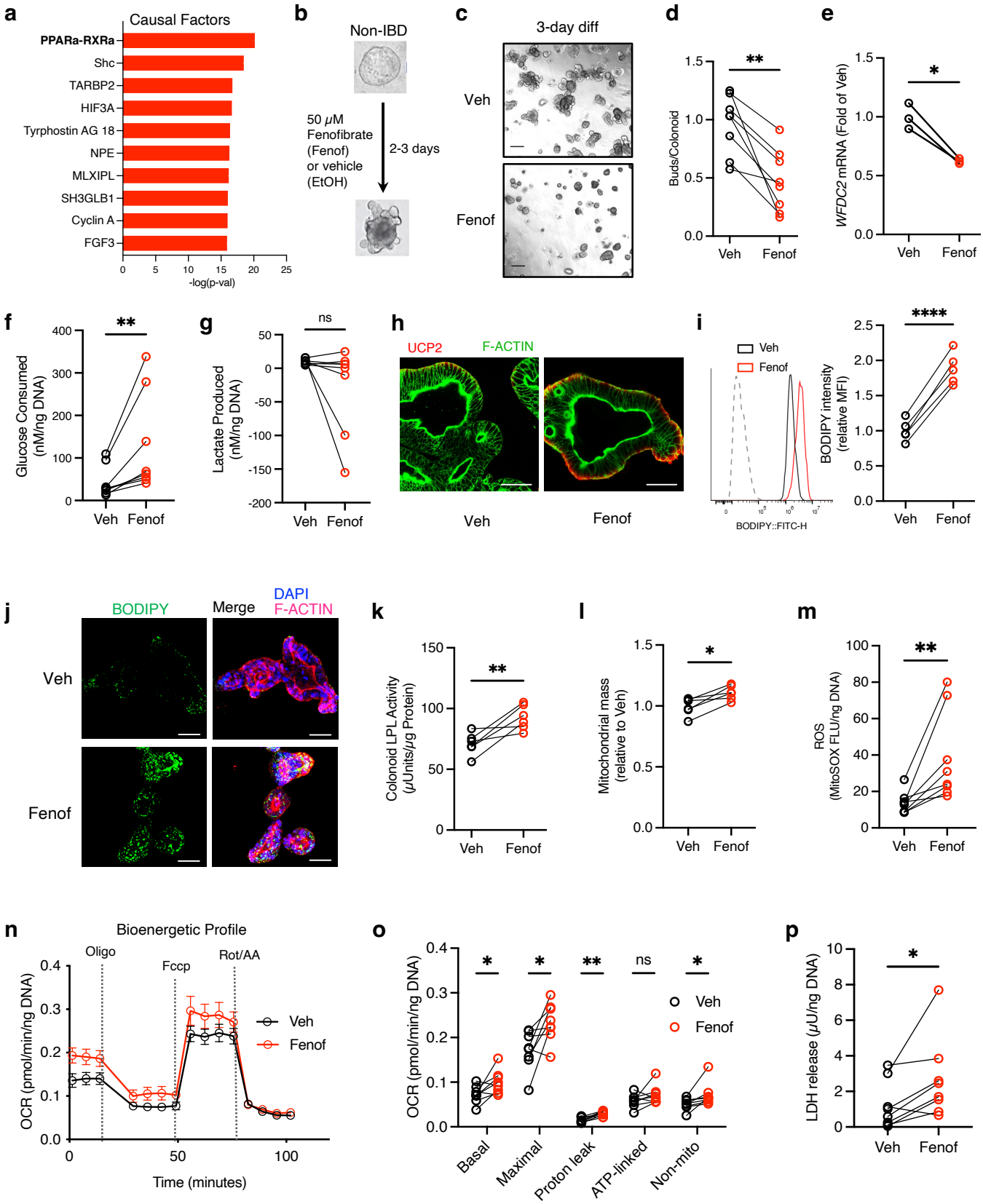
a
Causal Factors
PPARa-RXRa
Shc
TARBP2
HIF3A
Tyrphostin AG 18
NPE
MLXIPL
SH3GLB1
Cyclin A
FGF3
-log(p-val)
b
Non-IBD
50 μM Fenofibrate (Fenof) or vehicle (EtOH)
2-3 days
c
3-day diff
Veh
Fenof
d
Buds/Colonoid
Veh
Fenof
e
WFDC2 mRNA (Fold of Veh)
f
Glucose Consumed (nM/ng DNA)
g
Lactate Produced (nM/ng DNA)
ns
h
UCP2
F-ACTIN
i
BODIPY intensity (relative MFI)
BODIPY::FITC-H
j
BODIPY
Merge
DAPI
F-ACTIN
k
Colonoid LPL Activity (μUnits/μg Protein)
l
Mitochondrial mass (relative to Veh)
m
ROS (MitoSOX FLU/ng DNA)
n
Bioenergetic Profile
Oligo
Fccp
Rot/AA
OCR (pmol/min/ng DNA)
Time (minutes)
o
Basal
Maximal
Proton leak
ATP-linked
Non-mito
p
LDH release (μU/ng DNA)

1155

1156 **Fig. 5: PPAR-α agonism in non-IBD colonoids induces hypermetabolic stress during differentiation**
1157 **a**, Ingenuity Pathway Analysis of bulk transcriptomic data showing the top 10 predicted Causal Networks of
1158 differential gene expression between aUC and C colonoids. The full details of molecules involved under
1159 each master network are presented in Supplementary Table 4. **b**, Schematic of PPARA agonist, fenofibrate,
1160 treatment in non-IBD colonoids during differentiation. **c**, Representative phase contrast images of pediatric
1161 C colonoids treated as in **c**. Scale bar, 200 μm. **d**, The number of buds/colonoid in colonoids treated as in
1162 **b**, and differentiated for 3 days. Circles represent the average measures of individual colonoid lines**.** n=8
1163 patient colonoid lines/group, two-sided Wilcoxon signed-rank test. **e**, WFDC2 gene expression in colonoids
1164 treated as in **b**, assessed by qRT-PCR. Circles represent the average duplicate measures of individual
1165 colonoid lines**.** n=3 patient colonoid lines/group, two-sided paired t-test. **f**, Extracellular glucose and **g**,
1166 extracellular lactate concentration in 2-day ODM from C and aUC colonoids. Circles represent the average
1167 duplicate measures of individual colonoid lines relative to measures in blank wells with ODM only. n=8
1168 patient colonoid line/group, two-sided Wilcoxon signed-rank test. **h**, Representative confocal
1169 immunofluorescence images of UCP2 expression in non-IBD colonoids treated as in b, for 3 days. Scale
1170 bar, 50 μm **i**, Colonoids treated as in **b**, differentiated for 2 days and assayed for BODIPY$^+$ neutral lipid
1171 estimation by flow cytometry. Open symbols represent the mean fluorescence intensities (MFI) of BODIPY$^+$
1172 cells from individual patient colonoids, Data presented relative to the MFI of vehicle. n=5 patient lines/group,
1173 two-sided paired t-test. **j**, Representative confocal images of C colonoids treated as in **i**, for visualizing
1174 BODIPY$^+$ neutral lipid accumulation. Scale bar, 50 μm. **k**, LPL activity in C colonoids treated as in **b**, and
1175 differentiated for 2 days. Circles represent the average duplicate measures of individual colonoid lines. n=6
1176 patient colonoid lines/group, two-sided, paired t-test. **l**, Estimation of mitochondrial mass with Mitotracker
1177 green intensity in C colonoids treated as in **b**, and differentiated in ODM for 3 days. Circles represent the
1178 MFI of 5000 cells from individual colonoid lines relative to vehicle. n=8 patient spheroid line/group, two-
1179 sided paired t-test. **m**, C colonoids treated as in **b**, and differentiated for 3 days were used to estimate ROS
1180 with the MitoSOX fluorescence assay. Circles represent the average fluorescence of duplicate wells of
1181 individual colonoid lines**.** n=8 patient colonoid line/group, two-sided Wilcoxon signed-rank test. **n**,
1182 Bioenergetic profile of C colonoids treated as in **b**, and subjected to the Seahorse MitoStress test after a 3-
1183 day differentiation in ODM. Lines represent average OCR measures of individual colonoid lines. n=8 patient

1184 colonoid lines/group. **o**, MitoStress OCR responses of C colonoids in **n**, Circles represent the average
1185 quadruplicate wells of individual colonoid lines. n=8 patient colonoid line/group, two-sided paired t-test. **p**,
1186 LDH activity in ODM sampled from the same plate as **o** after a 2-day differentiation in ODM. Circles
1187 represent the average duplicate measures of individual colonoid lines. n=8 patient colonoid lines/group, two-
1188 sided Wilcoxon signed-rank test. n=8 colonoid lines/group. *=$P < 0.05$, **=$P < 0.01$, ***=$P < 0.001$. ****=$P <$
1189 0.0001 OCR, oxygen consumption rates; ODM, organoid differentiation medium
1190

Fig. 6

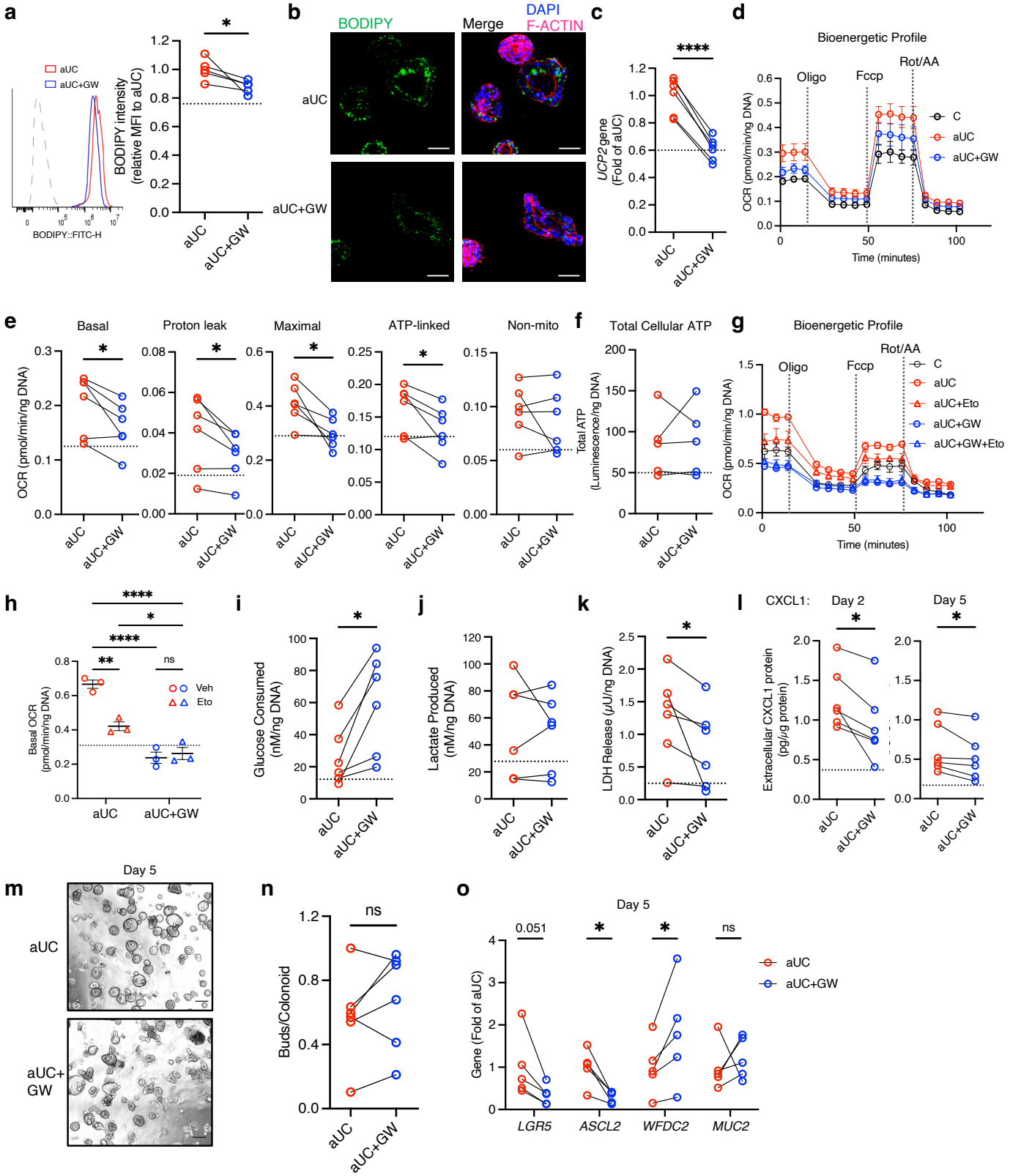
a
aUC
aUC+GW
BODIPY::FITC-H
BODIPY intensity (relative MFI to aUC)
b
BODIPY
Merge
DAPI
F-ACTIN
c
UCP2 gene (Fold of aUC)
d
Bioenergetic Profile
Oligo
Fccp
Rot/AA
OCR (pmol/min/ng DNA)
Time (minutes)
C
e
Basal
Proton leak
Maximal
ATP-linked
Non-mito
f
Total Cellular ATP
Total ATP (Luminescence/ng DNA)
g
aUC+Eto
aUC+GW+Eto
h
Basal OCR (pmol/min/ng DNA)
Veh
Eto
ns
i
Glucose Consumed (nM/ng DNA)
j
Lactate Produced (nM/ng DNA)
k
LDH Release (μU/ng DNA)
l
CXCL1:
Day 2
Day 5
Extracellular CXCL1 protein (pg/μg protein)
m
Day 5
aUC+ GW
n
Buds/Colonoid
o
Gene (Fold of aUC)
0.051
LGR5
ASCL2
WFDC2
MUC2

1191

1192 **Fig. 6: PPAR-α inhibition reprograms epithelial metabolism and ameliorates hypermetabolic stress**
1193 **in active UC colonoids during differentiation**
1194 aUC colonoids were treated with or without the PPAR-α antagonist, GW6471 (GW), during differentiation in
1195 ODM. **a**, GW effect on BODIPY$^+$ neutral lipid estimation by flow cytometry in aUC colonoids differentiated in
1196 ODM for 2 days. Open symbols represent the mean fluorescence intensities (MFI) of BODIPY$^+$ cells from
1197 individual patient colonoids. Data presented relative to the MFI of aUC controls. The dotted line indicates
1198 MFI of no stain control. n=5 patient lines/group, two-sided paired t-test. **b**, Representative confocal images
1199 of aUC colonoids treated as in **a**, for visualizing BODIPY$^+$ neutral lipid accumulation. Scale bar, 50 μm. **c**,
1200 Effect of GW on UCP2 gene expression by qRT-PCR. Open symbols represent the expression of individual
1201 colonoid lines. n=6 colonoid lines/group, two-sided paired t-test. **d**, Bioenergetic profile of aUC colonoids
1202 treated with or without GW and subjected to the Seahorse MitoStress test after a 3-day differentiation in
1203 ODM. Lines represent average OCR measures of individual colonoid lines. n=6 patient colonoid lines/group.
1204 **e**, MitoStress OCR responses of aUC colonoids treated as in **d**, Open circles represent the average
1205 quadruplicate wells of individual colonoid lines. n=6 patient colonoid line/group, two-sided paired t-test. The
1206 same colonoids cultured and used in **d**,**e**, were subjected to total ATP luminescence assay. Circles
1207 represent the average luminescence of duplicate wells of individual colonoid lines**.** n=6 patient colonoid
1208 line/group, two-sided Mann-Whitney test. **g**, Bioenergetic profile of aUC colonoids differentiated for 3 days
1209 in ODM with or without GW and subjected to the Seahorse MitoStress test in a nutrient-deprived medium
1210 with or without etomoxir. **h**, Basal OCR, aUC colonoids as in **g.** Symbols represent the average OCR from
1211 triplicate wells of individual colonoid lines. n=3 patient colonoid lines/group. 2-way ANOVA, Tukey's *post hoc*
1212 test. **i**, Extracellular glucose and **j**, lactate concentration in 2-day ODM from aUC colonoids with or without
1213 GW sampled from the same plate as **e**. Open circles represent the average duplicate measures of individual
1214 colonoid lines relative to measures in blank wells with ODM only. n=6 patient colonoid lines/group, two-
1215 sided Wilcoxon signed-rank test. **k**, LDH activity in ODM sampled from the same plate as **e** after a 2-day
1216 differentiation in ODM. Open circles represent the average duplicate measures of individual colonoid lines.
1217 n=6 patient colonoid lines/group, two-sided Wilcoxon signed-rank test. n=6 colonoid lines/group. **l,** aUC
1218 colonoids with or without GW were differentiated in ODM for 5 days. ODM collected on day 2 and on day 5
1219 (representing the last 3 days of differentiation) was used to assess CXCL1 secretion. Open circles

1220 represent the average duplicate measures of individual colonoid lines. n=6 patient colonoid lines/group, two-
1221 sided paired t-test. **m**, Representative phase contrast images of aUC colonoids differentiated in ODM with
1222 or without GW for 5 days. Scale bar, 200 μm. **n**. The number of buds/colonoid in aUC colonoids treated as
1223 in **m**. Open circles represent the average measures of individual colonoid lines**.** n=6 patient colonoid
1224 lines/group, two-sided Wilcoxon signed-rank test. **o**, Effect of GW on gene expression of differentiation
1225 markers assessed by qRT-PCR. Open symbols represent the expression of individual colonoid lines. n=6
1226 colonoid lines/group, two-sided paired t-test. Dotted vertical lines represent the average of at least 2 non-
1227 IBD control colonoids. *=$P < 0.05$, **=$P < 0.01$, ***=$P < 0.001$. ****=$P < 0.0001$ OCR, oxygen consumption
1228 rates; ODM, organoid differentiation medium
1229
1230

1231 **Extended data**

1232

Extended Data Fig. 1

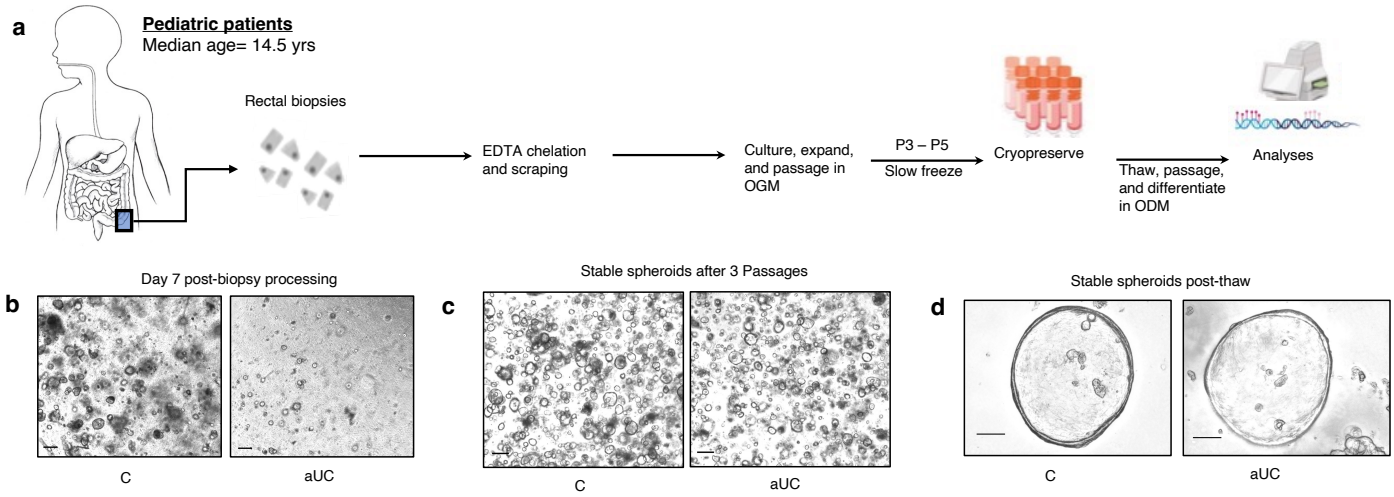

1233

1234 **Extended Data Fig. 1: Colon Epithelial Spheroid Generation**

1235 **a**, Schematic of epithelial spheroids derivation and maintenance from pediatric rectal biopsies.
1236 Demographics of pediatric patients are provided in Supplementary Table 1. **b**, Phase-contrast images of C
1237 and aUC spheroids after the first 7 days of biopsy derivation in OGM show that the development of aUC
1238 spheroids from biopsies is slower than the C spheroids. Scale bar, 200 μm**. c**, Phase contrast images of C
1239 and aUC spheroids in culture after 3 passages, showing that after initial slow growth rates, aUC spheroids
1240 become more stable like C spheroids. Scale bar, 200 μm. **d**, High magnification images of C and aUC
1241 spheroids, showing expected morphology with large lumens after freeze-thaw protocol. Scale bar, 50 μm.
1242 OGM, Organoid Growth Medium; ODM, Organoid Differentiation Medium

1243

Extended Data Fig. 2

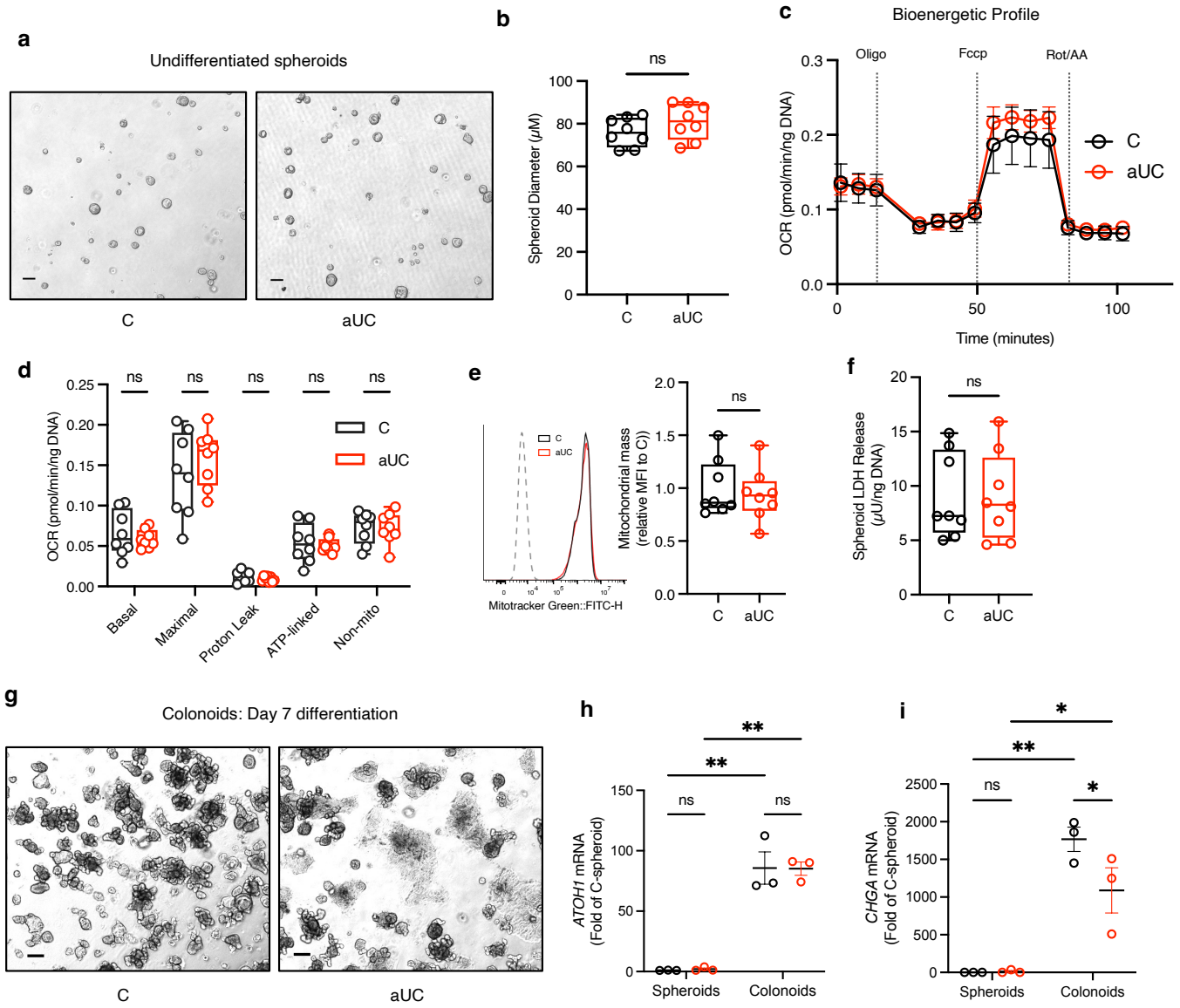

Extended Data Fig. 2: Pediatric colon spheroids exhibit similar morphological and metabolic profiles **a**, Phase contrast images of undifferentiated C and aUC spheroids filtered after trypsinization, passed through a strainer, and monitored for 7 days. Scale bar, 200 μm. **b**, Diameter of C and aUC spheroids described in **a.** Blinded measures of the diameter of all spheroids on a high-powered field were taken. Black and Red circles represent the average measures of individual spheroids within a high-powered field of each spheroid line**.** n=8 patient spheroid line/group, two-sided Mann-Whitney test. **c**, Bioenergetic profile of C and aUC spheroids from Seahorse MitoStress test. n=8 patient spheroid line/group. Black and Red lines represent average OCR measures of individual spheroid lines. **d**, OCR response of C and aUC spheroids

1253 cultured in unstimulated conditions in OGM. Black and Red circles represent the average quadruplicate
1254 wells of individual spheroid lines. n=8 patient spheroid line/group, unpaired, two-sided t-test. **e**, Estimation of
1255 mitochondrial mass with Mitotracker green intensity in undifferentiated C and aUC spheroids. Black and
1256 Red circles represent the mean fluorescence intensities (MFI) of 5000 cells from individual spheroid lines.
1257 n=8 patient spheroid line/group, two-sided Mann-Whitney test. **f**, LDH activity in C and aUC spheroids in
1258 OGM from the same plate as **c**, **d**. Black and Red circles represent the average duplicate measures of
1259 individual spheroid lines. n=8 patient spheroid line/group, unpaired, two-sided t-test. **g**, Phase contrast
1260 images of C and aUC differentiated spheroids (colonoids) on day 7 of differentiation. Scale bar, 200 μm. **h**,
1261 Spheroids embedded in Matrigel were cultured in OGM and paired samples were differentiated in ODM for
1262 3 days (colonoids) and assay for **h**, *ATOH1* and **i**, *CHGA* mRNA abundance using qRT-PCR. n=3 patient
1263 line/group, 2-way ANOVA. *=$P < 0.05$, **=$P < 0.01$. OCR, oxygen consumption rates; ODM, organoid
1264 differentiation medium; OGM, organoid growth medium
1265
1266

Extended Data Fig. 3

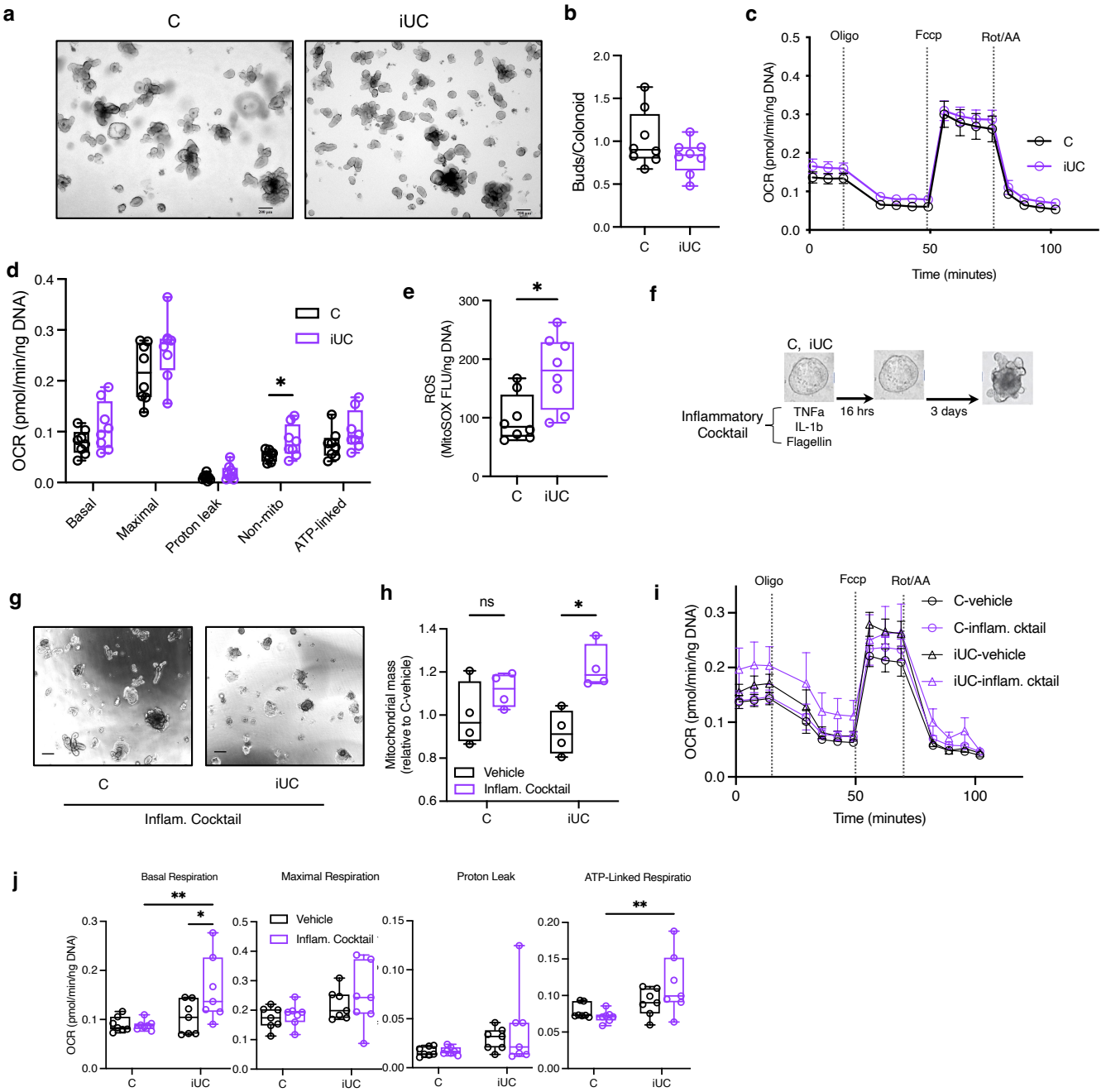

Extended Data Fig. 3: Colonoids from patients with inactive UC exhibit increased metabolic susceptibility to inflammatory stimulus.

a, Phase contrast images of pediatric C and iUC colonoids after 3-day differentiation in unstimulated conditions in ODM. Scale bar, 200 µm. **b**, The number of buds/colonoid in colonoids treated as in **a**. Black and purple circles represent the average measures of individual colonoid lines**.** n=8 patient colonoid line/group, two-sided Mann-Whitney test. **c**, Bioenergetic profile of C and iUC colonoids differentiated for 3

1274 days as in **a**, and subjected to the Seahorse MitoStress test. Black and Purple lines represent average OCR
1275 measures of individual colonoid lines. n=8 patient colonoid line/group. **d**, MitoStress OCR response of C
1276 and iUC colonoids differentiated for 3 days as in **a**, in 96-well Seahorse plate. Black and Purple circles
1277 represent the average quadruplicate wells of individual colonoid lines. n=8 patient colonoid line/group,
1278 Mann-Whitney test. **e**, The same cohort of colonoids cultured and used in **d**, were used to estimate
1279 mitochondrial ROS with the MitoSOX fluorescence assay. Black and Purple circles represent the average
1280 fluorescence of duplicate wells of individual colonoid lines**.** n=8 patient colonoid line/group, two-sided Mann-
1281 Whitney test. **f**, C, and iUC spheroids were exposed to an inflammatory cocktail (40 ng/mL TNFa, 20 ng/mL
1282 IL-1b, and 500 ng/mL Flagellin) in OGM for 16 hrs before differentiation in ODM for 3 days. **g**, Phase
1283 contrast images of C and iUC colonoids treated as in **f**. Scale bar, 200 μm. **h**, Estimation of mitochondrial
1284 mass with Mitotracker green intensity in C and iUC colonoids treated as in **f**. Black and purple circles
1285 represent the mean fluorescence intensities (MFI) of 5000 cells from individual spheroid lines. n=4 patient
1286 colonoid line/group, 2-way ANOVA, with Tukey correction. **i**, Bioenergetic profile of C and iUC colonoids
1287 treated as in **f**, and subjected to the Seahorse MitoStress test. Black and Purple lines represent average
1288 measures of individual colonoid lines. n=4 patient colonoid line/group. **j**, MitoStress OCR response of C and
1289 iUC colonoids treated as in **f**. Black and Purple circles represent the average quadruplicate wells of
1290 individual colonoid lines. n=7 patient colonoid line/group, 2-way ANOVA with Tukey correction. *=$P < 0.05$,
1291 **=$P < 0.01$, ***=$P < 0.001$. OCR, oxygen consumption rates; ODM, organoid differentiation medium; OGM,
1292 organoid growth medium; ROS, reactive oxygen species
1293

Extended Data Fig. 4

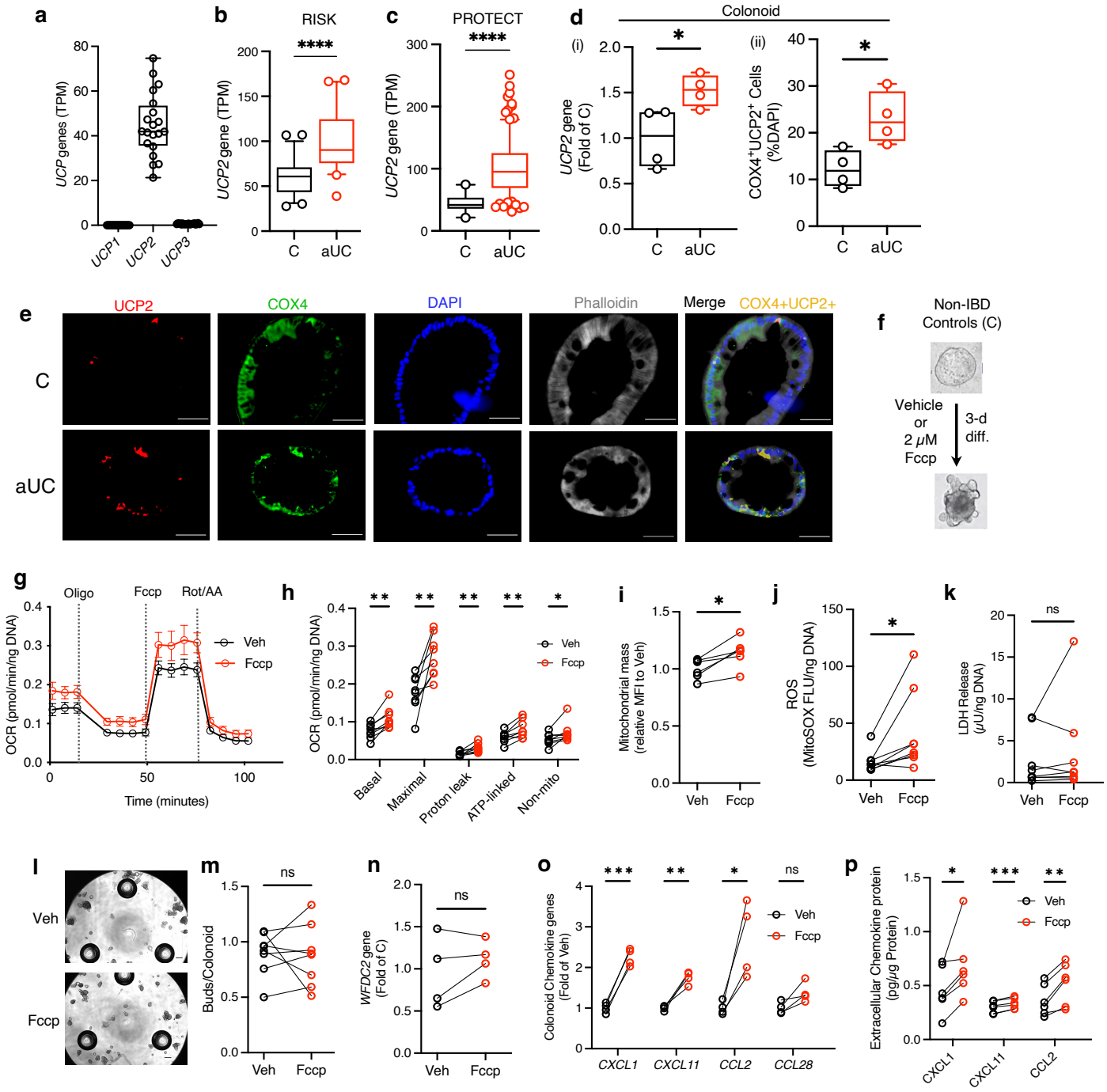

Extended Data Fig. 4: Metabolic uncoupling contributes to hypermetabolic phenotypes during colonoid differentiation

a, Rectal gene expression of uncoupling proteins in bulk RNA-Seq data from non-IBD control participants in the NIH PROTECT study showing dominant UCP2 gene expression over other uncouplers (transcripts per million (TPM) values). n=20. **b**, Rectal UCP2 gene expression (TPM) from treatment-naïve participants with

1300 UC in the RISK cohort. n=43-55/group. Two-tailed Mann-Whitney test. **c**, Rectal UCP2 gene expression
1301 (TPM) from the NIH PROTECT study of treatment-naive pediatric UC patients. n=20(C) -206(aUC) /group.
1302 Two-tailed Mann-Whitney test. **d**, (i) UCP2 gene expression assessed by qRT-PCR and (ii) UCP2 protein
1303 expression in pediatric C and aUC colonoids differentiated for 3 days in ODM. n=4 patient colonoid
1304 line/group i) two-tailed unpaired t-test. ii) two-sided Mann-Whitney test. **e,** C and aUC colonoids were
1305 embedded in OCT after 3-day differentiation. Representative immunofluorescence images showing UCP2
1306 expression and merged expression with the mitochondrial marker, COX4. Semi-quantitation of
1307 COX4+UCP2+ cell counts is presented in d(ii). Scale bar, 50 μm. **f**, Morphological and metabolic effects of
1308 mitochondrial uncoupling during colonoid differentiation were tested in C colonoids treated with or without
1309 the mitochondrial protonophore, FCCP. **g**, Bioenergetic profile of C colonoids treated as in **f**, and subjected
1310 to the Seahorse MitoStress test. Black and Red lines represent average OCR measures of individual
1311 colonoid lines. n=8 patient colonoid lines/group. **h**, MitoStress OCR response of C colonoids treated as in **f**,
1312 in 96-well Seahorse plate. Black and Red circles represent the average quadruplicate wells of individual
1313 colonoid lines. n=8 patient colonoid line/group, two-sided paired t-test. **i**, Estimation of mitochondrial mass
1314 with Mitotracker green intensity in C colonoids treated as in **f**. Black and Red circles represent the mean
1315 fluorescence intensities (MFI) of 5000 cells from individual colonoid lines. n=8 patient spheroid line/group,
1316 two-sided paired t-test. **j**, The same set of colonoids cultured and used in **f**, were used to estimate
1317 mitochondrial ROS with the MitoSOX fluorescence assay. Black and Red circles represent the average
1318 fluorescence of duplicate wells of individual colonoid lines**.** n=8 patient colonoid line/group, two-sided
1319 Wilcoxon signed-rank test. **k**, LDH activity in ODM taken from the same plate as **h** after a 2-day
1320 differentiation. Black and Red circles represent the average duplicate measures of individual colonoid lines.
1321 n=8 patient colonoid lines/group, two-sided Wilcoxon signed-rank test. **l**, Representative phase contrast
1322 images of pediatric C colonoids treated as in **f**. Scale bar, 200 μm. **m**, The number of buds/colonoid in
1323 colonoids treated as in **f**. Black and Red circles represent the average measures of individual colonoid lines**.**
1324 n=8 patient colonoid line/group, two-sided Wilcoxon signed-rank test. **n**, WFDC2 gene expression in
1325 colonoids treated as in **f**, assessed by qRT-PCR. Black and Red circles represent the average measures of
1326 individual colonoid lines**.** n=4 patient colonoid lines/group, paired t-test. **o**, Gene expression of chemokines
1327 in colonoids treated as in **f**, assessed by qRT-PCR. Black and Red circles represent the average measures

of individual colonoid lines**.** n=4 patient colonoid line/group, paired t-test. **p**, Colonoids were treated as in **f**, and Chemokine protein concentrations were assessed in ODM after a 2-day differentiation. Black and Red circles represent the average duplicate measures of individual colonoid lines. n=6 colonoid lines/group, paired t-test. *=$P < 0.05$, **=$P < 0.01$, ***=$P < 0.001$. LDH, lactate dehydrogenase; OCR, oxygen consumption rates; ODM, organoid differentiation medium; ROS, reactive oxygen species

Extended Data Fig. 5

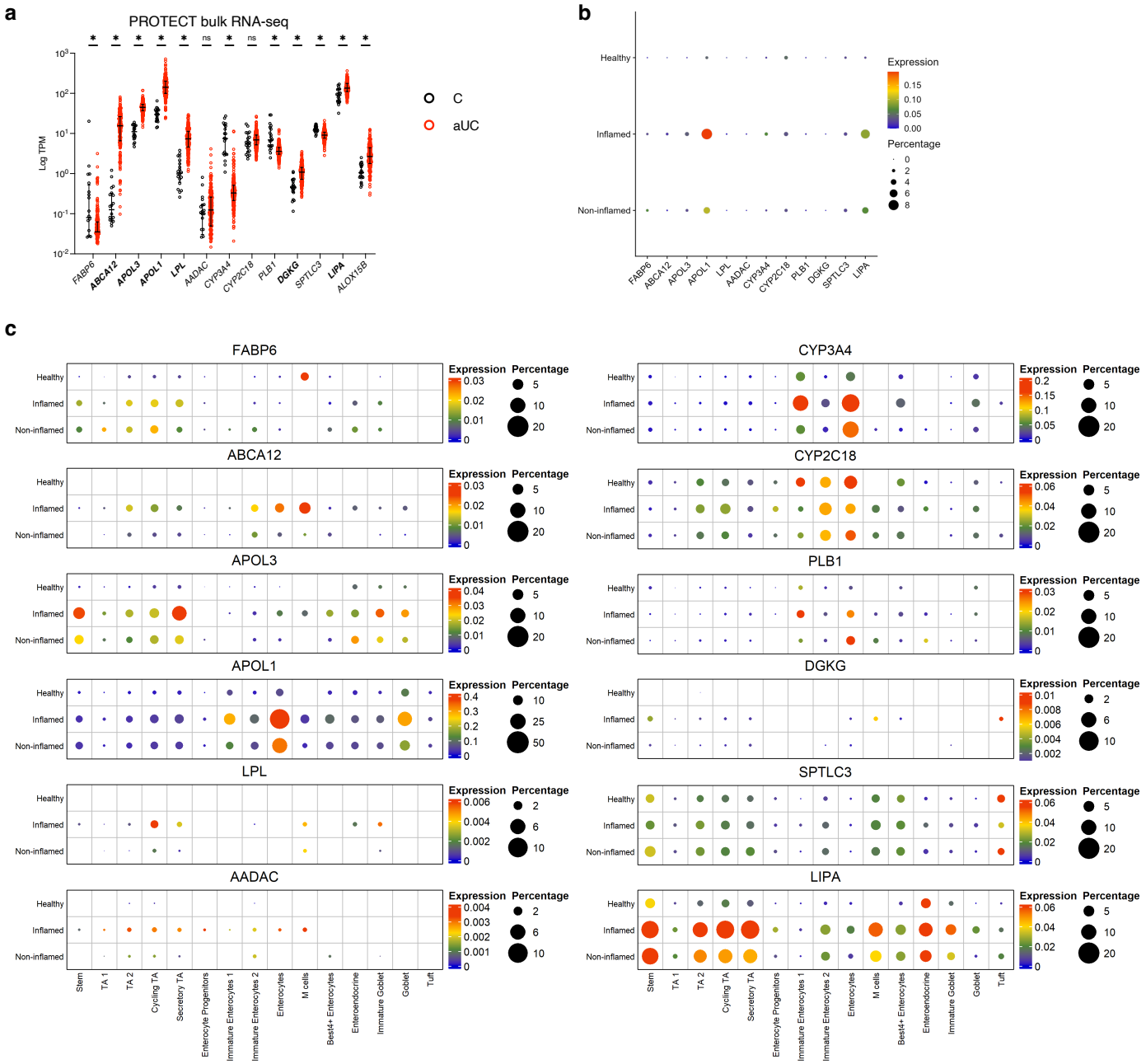

1335 **Extended Data Fig. 5: Dysregulated lipid metabolism genes in the colon epithelia of active UC**

1336 **a**, Rectal gene expression (TPM) of lipid-related colonoid genes (as in Fig. 4**a**) from the NIH PROTECT

1337 study[19] of treatment-naive pediatric UC patients. n=20(C) -206(aUC)/group. Kruskal-Wallis test with Dunn's

1338 multiple comparisons. Black and Red symbols represent the TPM value of each patient's data. **b**,

1339 Expression of colonoid lipid-related genes (as in Fig. 4**a**) by disease state in publicly available adult single-

1340 cell (sc) RNA-seq data[39]. Data is colored by relative gene expression and the relative size of each dot

1341 shows the percentage of cells expressing each marker per disease state. **c**, Expression of colonoid lipid-

1342 related genes (as in Fig. 4**a**) in scRNA-seq data[39] by epithelial cluster. Data is colored by relative gene

1343 expression and the relative size of each dot shows the percentage of cells expressing each marker per

1344 epithelial cluster.*=$P < 0.05$, **=$P < 0.01$, ***=$P < 0.001$.

1345

1346

Extended Data Fig. 6

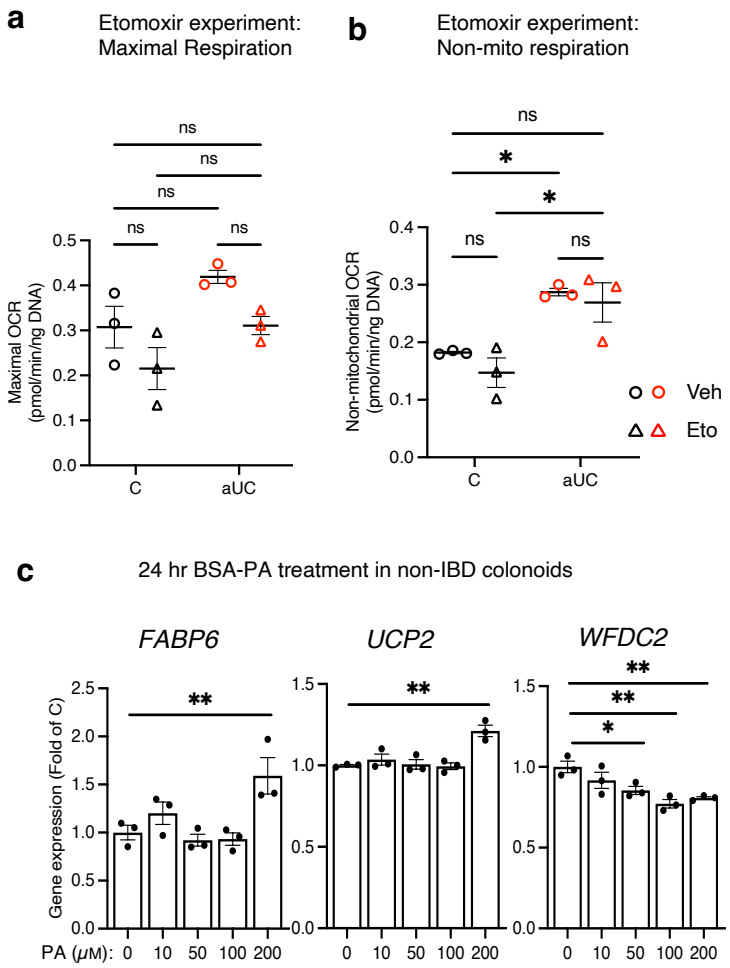

Extended Data Fig. 6: Lipotoxicity modulates UCP2 and WFDC2 gene expression during differentiation

a, Maximal respiration and, **b**, Non-mitochondrial respiration of C, and aUC colonoids differentiated for 3 days in ODM and subjected to the Seahorse MitoStress test in a nutrient-deprived medium with or without Etomoxir. Black and Red symbols represent the average OCR from triplicate wells of individual colonoid lines n=3 patient colonoid lines/group. 2-way ANOVA, Tukey's *post hoc* test. **c**, qRT-PCR gene expression data of non-IBD colonoids differentiated in ODM for 24 hrs with the stated doses of BSA-PA. Symbols represent 3 technical replicates in independent matrigel domes. One-way ANOVA and Dunnett tests. *=$P < 0.05$, **=$P < 0.01$. BSA, bovine serum albumin; OCR, oxygen consumption rates; ODM, organoid differentiation medium; PA, Palmitic acid

Extended Data Fig. 7

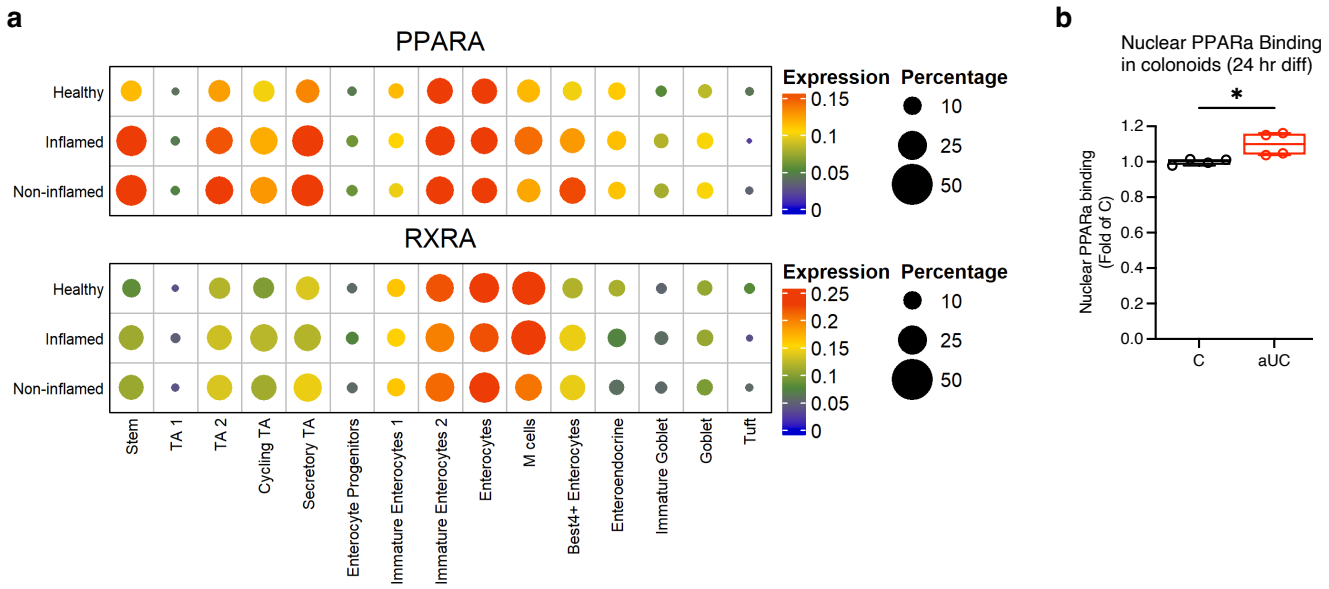

Extended Data Fig. 7: Epithelial PPARA expression in active UC

a, Colon scRNA-seq data[39] showing the expression of PPARA and RXRA by disease state in colon epithelial lineages. Data is colored by relative gene expression and the relative size of each dot shows the percentage of cells expressing each marker per disease state. **b**, PPAR-α activity assay in nuclear extracts of pooled C and aUC colonoids (n=3/group) differentiated for 24 hrs. Black and red symbols represent four technical replicates from pooled nuclear extracts and are presented relative to C. Two-sided unpaired t-test. *=$P < 0.05$.

Extended Data Fig. 8

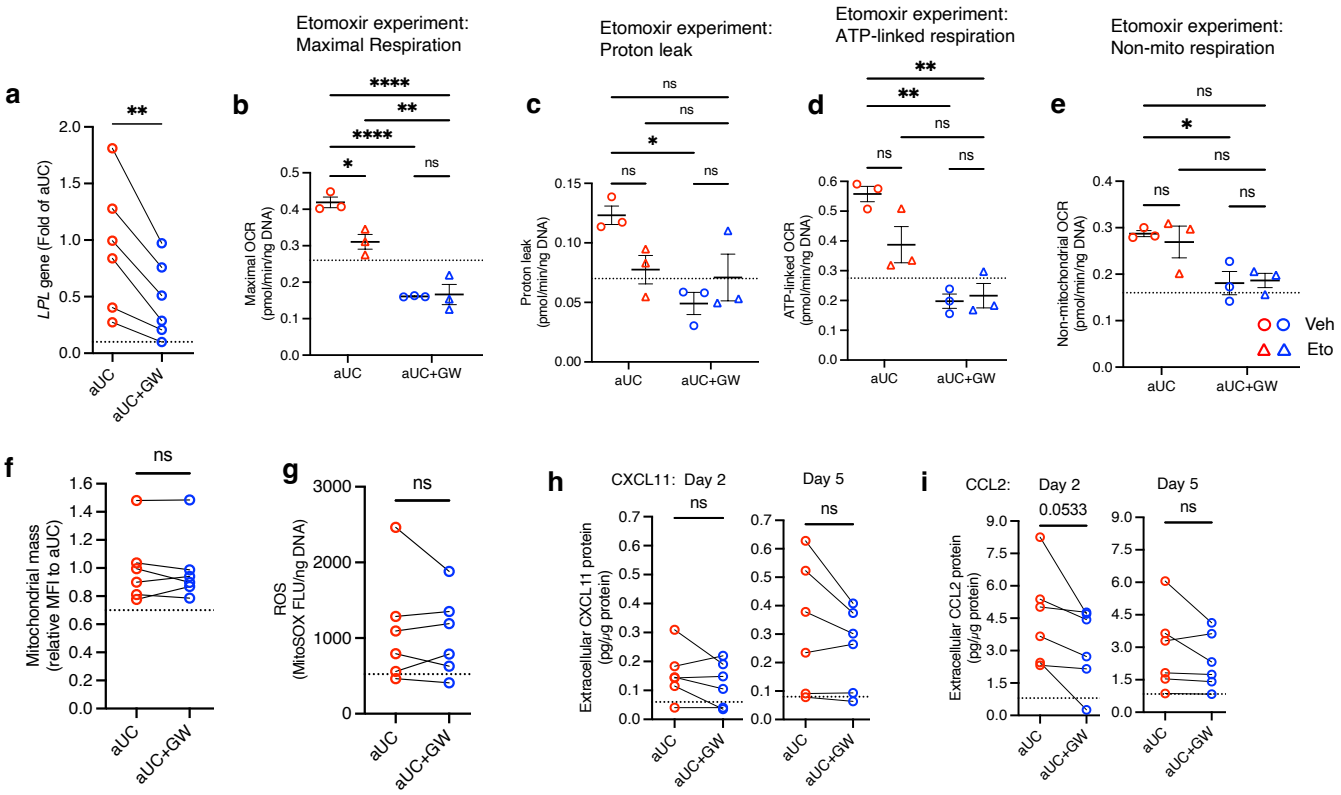

Extended Data Fig. 8: Blockade of lipid synthesis suppresses hypermetabolic features in active UC colonoids

aUC colonoids were treated with or without the PPAR-α antagonist, GW6471 (GW), during differentiation in ODM. **a**, Effect of GW on *LPL* gene expression by qRT-PCR. Red and Blue open circles represent the expression of individual colonoid lines. n=6 colonoid lines/group, two-sided paired t-test. **b**, Maximal, **c**, Proton leak **d**, ATP-linked, and **e**, Non-mitochondrial OCR response of aUC colonoids differentiated for 3 days in ODM with or without GW and subjected to the Seahorse MitoStress test in a nutrient-deprived medium with or without Etomoxir. Red and Blue symbols represent the average OCR from triplicate wells of individual colonoid lines. n=3 patient colonoid lines/group. 2-way ANOVA, Tukey's *post hoc* test. **f**, Estimation of mitochondrial mass with Mitotracker green intensity in aUC colonoids treated with or without GW in ODM for 3 days. Red and Blue open circles represent the MFI of 5000 cells from individual colonoid lines relative to aUC. n=6 patient spheroid line/group, two-sided Wilcoxon signed-rank test. **g**, ROS estimate with the MitoSOX fluorescence assay in a UC colonoids differentiated for 3 days with or without GW. Red and Blue open circles represent the average fluorescence of duplicate wells of individual colonoid lines**.** n=6

1383 patient colonoid line/group, two-sided Wilcoxon signed-rank test. **h,** aUC colonoids with or without GW were
1384 differentiated in ODM for 5 days. ODM collected on day 2 and on day 5 (representing the last 3 days of
1385 differentiation) was used to assess CXCL11 and **i**, CCL2 secretion. Red and Blue open circles represent the
1386 average duplicate measures of individual colonoid lines. n=6 patient colonoid lines/group, two-sided paired
1387 t-test. *=$P < 0.05$, **=$P < 0.01$, ***=$P < 0.001$. ****=$P < 0.0001$ OCR, oxygen consumption rates; ODM,
1388 organoid differentiation medium; MFI, mean fluorescence intensity
1389
1390
1391 **Supplementary information**
1392
1393 Supplementary Table 1: Patient demographics *(Microsoft Word)*
1394
1395 Supplementary Table 2: Colonoid Bulk RNA-seq. *(Microsoft Excel file)*
1396
1397 Supplementary Table 3: Ingenuity Pathway Analysis: Molecular and Cellular Functions *(Microsoft Excel file)*
1398
1399 Supplementary Table 4: Ingenuity Pathway Analysis: Causal Networks *(Microsoft Excel file)*
1400
1401 Supplementary Table 5: Taqman Probes for qRT-PCR *(Microsoft Word file)*